FLUVIAL ARCHITECTURAL ANALYSIS AND LONGITUDINAL VARIANCE OF THE CASTLEGATE SANDSTONE, BOOK CLIFFS, UTAH

By

BRAYTON KEITH

Bachelor of Science in Geology, 2021
University Alaska, Anchorage
Anchorage, AK

Submitted to the Graduate Faculty of The
College of Science and Engineering
Texas Christian University
in partial fulfillment of the requirements
for the degree of

Master of Science in Geology

May 2025

FLUVIAL ARCHITECTURE ANALYSIS AND LONGITUDINAL VARIANCE OF THE CASTLEGATE SANDSTONE, BOOK CLIFFS, UTAH

by

Brayton Keith

Thesis approved:

Major Professor

For the College of Science and Engineering

Acknowledgements

A massive thank you to Dr. John Holbrook for being an amazing mentor and teacher who encouraged me to be great, be skeptical, and was always there to talk through my conceptual questions and lead me to my own answer. Thank you to my committee members, Bo Henk and Arthur Busbey for your time and help in the revision process. Thank you to Dr. William Little and Dr. Jennifer Aschoff for your recommendations in the search for the best outcrops. Thank you to all of my classmates Henry Henk, Payton O'Brien, and Sam Knox who helped me in the field, and being there for discussions on theories and hypotheses. Thank you to everyone who gave me advice and offered valuable discussion on my work at various conferences. I would like to thank my family for their encouragement and support throughout all of the ups and downs of life. Thank you, mom, for reminding me of my love for geology, and encouraging me to pursue this field as a degree and career path that you knew I would enjoy. Thank you to my father and grandfather, as the two of you taught me hard work, and the very important lesson to take pride in any and all work that I do, as that simple lesson shaped my approach and integrity to always do my best. And to my little sister, Brenna, thank you for always being there for me.

TABLE OF CONTENTS

Acknowledgements ii

List of Figures iv

List of Tables vi

CHAPTER ONE: Introduction 1

1.1) Tectonic Setting 2

1.2) Climate 5

1.3) Stratigraphy 6

CHAPTER TWO: Methods 15

CHAPTER THREE: Results 20

3.1) Architecture 20

3.2) Backwater Length 61

CHAPTER FOUR: Discussion 63

4.1) Trackable Surfaces 64

4.2) Valleys at Woodside Canyon 71

4.3) Climate 78

CHAPTER FIVE: Conclusions 80

References 82

VITA

ABSTRACT

List of Figures

Figure 1: Map of structural components 4

Figure 2: U-Pb parent groups of Castlegate rivers 8

Figure 3: Castlegate sequence stratigraphic models 11

Figure 4: Blakey map of the Middle Campanian 14

Figure 5: Outcrop locations in modern Book Cliffs 16

Figure 6: Idealized unstable antidune bedforms 22

Figure 7: Salina Canyon orthomosaic, surfaces, and architecture 23

Figure 8: Salina upper-flow regime bedforms 24

Figure 9: Joe's Valley Reservoir orthomosaic, surfaces, and architecture 28

Figure 10: Gravel bar, Joe's Valley Reservoir 29

Figure 11: Castlegate type-section orthomosaic, surfaces, and architecture 33

Figure 12: Sunnyside Canyon orthomosaic, surfaces, and architecture 37

Figure 13: Woodside Canyon orthomosaic, surfaces, and architecture 42

Figure 14: Crescent Canyon orthomosaic, surfaces, and architecture 46

Figure 15: West Blaze Canyon orthomosaic, surfaces, and architecture 50

Figure 16: Thompson Canyon orthomosaic, surfaces, and architecture 54

Figure 17: Bayhead delta depositional model 57

Figure 18: Sulfur Canyon orthomosaic, surfaces, and architecture 59

Figure 19: Longitudinal profile of outcrop belt 63

Figure 20: Orthomosaics on plainview map 70

Figure 21: Backwater length, knickpoint migration, shoreline trajectories 77

List of Tables

Table 1: Outcrop locations.....15

Table 1: Backwater length and relevant data.....62

CHAPTER ONE: Introduction

The Castlegate Sandstone is among the most studied fluvial deposits in the world due to its world-class longitudinal continuity of outcrop, and for being frequently visited for siliciclastic sequence stratigraphic research and educational purposes. Despite this, there has yet to be a large-to-fine scaled, comprehensive fluvial architectural element analysis study completed on the Castlegate Sandstone that consider the longitudinal variance within the system. Fluvial architecture studies within the Castlegate have typically focused on single sites within the system (i.e. proximal, medial, distal), and architectural elements smaller than valley-scale incisions (Channel and bar forms), or larger-scale surfaces such as sequence boundaries. These studies have not compared outcrop within the longitudinal section across architectural hierarchies, resulting in miles of outcrop being left yet to interpretation.

This study aims to provide a more comprehensive architectural analysis of the Castlegate Sandstone with focus on vertical and dip-oriented shifts in facies and architectural style within the system, using outcrop orthomosaics with architectural interpretations. Orthomosaics used herein represent an ~180 km down-dip longitudinal profile. More importantly, this study aims to add focus to the valley and multi-valley scale bounding surfaces internal to the Castlegate, which have been largely overlooked. The use of orthomosaics allows for the opportunity to view outcrop on a scale that may allow for high width:thickness ratio channel belts and valleys to be observed and interpreted, where in outcrop measurements they are easily overlooked. This study aims to determine the following:

1. Presence or lack thereof of valley and multi-valley scale incisions throughout the Castlegate outcrops

2. Variability in channel styles and patterns up and down-dip
3. Up-dip to down-dip variation in incision and aggradation in the Castlegate fluvial system and possible correlation of incisional patterns
4. Possible driving factors of variation in fluvial style and incisional patterns longitudinally

1.1) Tectonic Setting

The onset of the Sevier Orogeny, resultant of subduction of the Farallon plate beneath the North American plate, led to uplift and subsequent deposition of sediment during the Late Cretaceous Campanian into the Cretaceous Western Interior Seaway of the Cordilleran retroarc-foreland basin (Lawton, 1986; Robinson & Slingerland, 1998; Aschoff & Steel, 2011). Sedimentation in the basin was primarily from W-NW to E-SE during deposition of the Blackhawk Formation and Castlegate Sandstone (Aschoff & Steel, 2011), sourced from uplifted topography of the Sevier Orogen to the West (Armstrong, 1968; Aschoff & Steel, 2011). Sediment in the area fed from three localized uplifts, from Charleston-Nebo Thrust Belt to the North, the Canyon Range, and the Pavant Thrust belts to the South (Figure 1; Armstrong, 1968; Lawton, 1986; Horton et al., 2004; DeCelles & Coogan, 2006). The onset of transition from Sevier to Laramide-style deformation began in central Utah at ~ 77 Ma (Aschoff & Steel, 2011), and recent provenance analysis places the deposition of the upper Blackhawk Formation and entirety of the Castlegate Sandstone at its type-section to 77-75.01 Ma with the entirety of the Castlegate deposited between 76 to 75 Ma (Pettit et al, 2019). This new age constraint has implications for the deformation style during Castlegate deposition and thus implications for syndepositional subsidence and uplift in the system, with possible influence of shorter wavelength deformation coincident with the transition to

Laramide-style deformation (Aschoff & Steel, 2011). Post-deposition, uplift of the Colorado Plateau in the Neogene led to uplift of the Campanian strata of the Book Cliffs with nearly no deformation, faulting, and very little tilting of these rocks. This preserves these strata as a continuous, undeformed outcrop belt with continuous dip-oriented outcrop and plentiful canyons providing strike-oriented outcrop views. This trend of exposure has made the Castlegate Sandstone a popular target for sequence stratigraphic education and study (e.g. Van Wagoner et al. 1990; Van Wagoner 1991, 1995; Miall 1993, 1994, 2014, 2016; Yoshida et al. 1996, 1998; McLaurin & Steel 2000, 2007; Willis 2000; Yoshida 2000; Miall & Arush 2001a, 2001b; Hettinger and Kirschbaum 2002; Hampson 2010, 2016; Seymour & Fielding 2013; Hampson et al. 2014; Pattison, 2018, 2019a, 2019b, 2020).

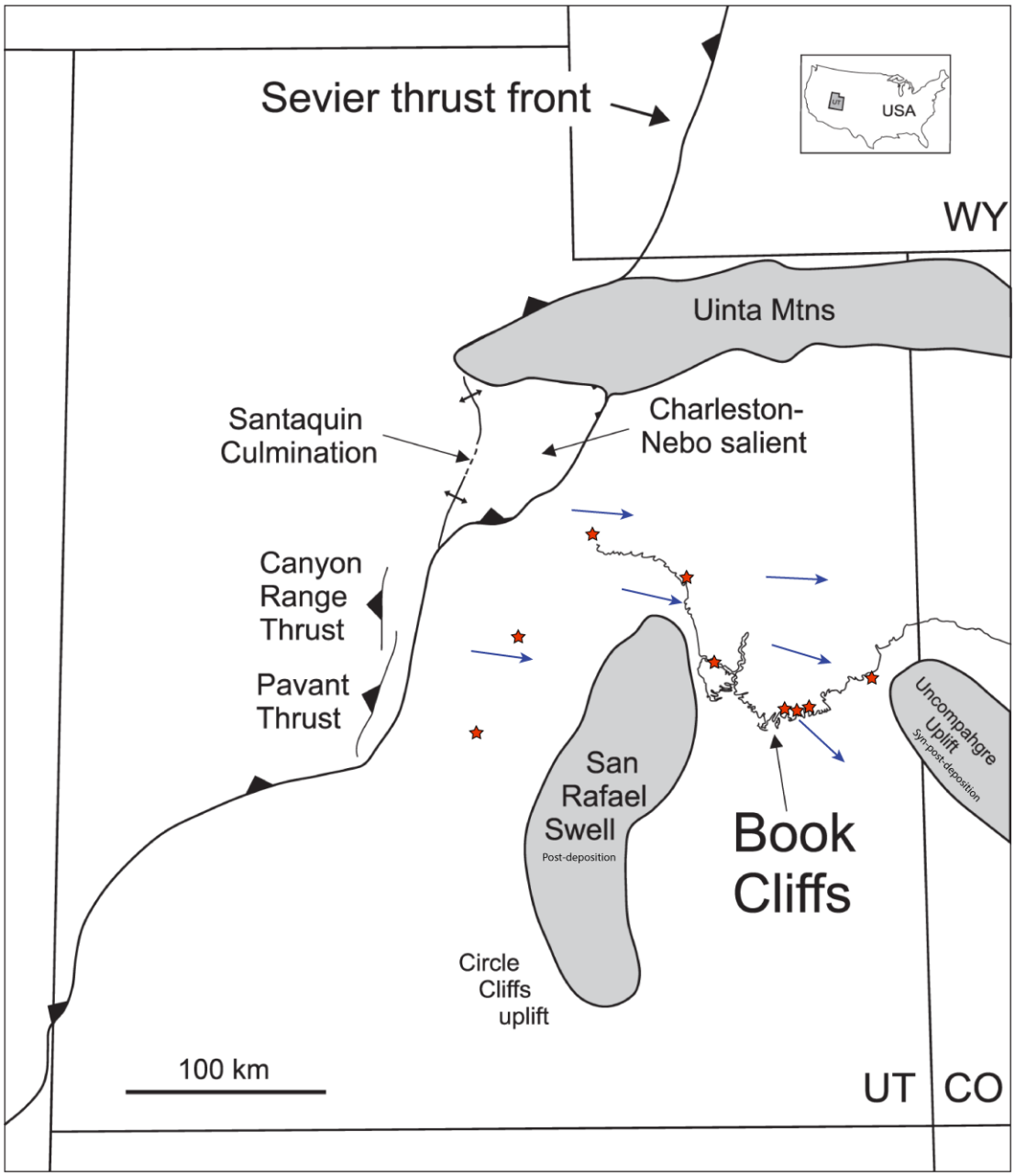

***Figure 1*:** Map of structural features in the study area (modified from Pattison, 2018; Horton et al. 2004). Red stars represent outcrop locations used in this study and their locations relative to different structural components. Blue arrows represent sediment routing from the lower, sandy amalgamated deposits of the Castlegate Sandstone (Miall, 2001). San Rafael Swell is uplifted after Castlegate deposition. Uncompahgre Uplift may have been active during part, or all of Castlegate deposition. Note that each proximal outcrop is fed by a different thrust front, with sediment in Salina Canyon sourced from the Pavant Thrust, Joe's Valley Reservoir from the Canyon Range Thrust, and the Castlegate Type-section sourced from the Charleston-Nebo Salient due to their distinct U-Pb signatures (Pettit et al., 2019).

1.2) Climate

The Castlegate Sandstone of the late Campanian was deposited at a paleo-latitude of ~47° N (Miller et al., 2013). Multiple model simulations (Poulsen et al., 2007; Fricke et al., 2010; Sewall & Fricke, 2013; Kump & Slingerland, 1999; Poulsen et al., 1999) and Δ_{47} analysis of carbonate materials such as paleosol nodules, bivalves, and macrofossils (Dennis et al., 2013; Foreman et al., 2011; Fricke et al., 2010) have all indicated that the western margin of the Western Interior Seaway (WIS) had highly seasonal climate with increased precipitation in summer months owing to a strongly monsoon-driven climate during the Campanian. Further analysis of $\delta^{18}O$ data and strontium isotopes from fluvial channels in the late Campanian Kaiparowits Formation of southern Utah both reinforce the monsoonal model (Curley et al., 2025). Analysis of alluvial micritic carbonate muds in the late Campanian Kaiparowits Formation (~75 ma) suggest a mean temperature ($T(\Delta_{47})$) of 35 ± 4 °C during the warmest months and ~2 to ~10 °C for the coldest months of the year (Burgener et al., 2019). This study implies a high variability in temperature from winter to summer months during the deposition of late Campanian strata of the WIS with mean annual range in temperature of ~21 to ~29 °C (Burgener et al., 2019). $\delta^{18}O$ data for low and high latitude outcrops of in the late Campanian (~75 ma) estimates mean elevations of ≥3975 m in the Cordilleran highlands (Curley et al., 2025). This data indicates a strong effect of seasonality with high elevations. This argues for a strong rain-shadow effect likely occurring at the headwaters, resulting in high variability in precipitation and river discharge during the deposition of the Castlegate Sandstone due to high temperature variance during the interpreted strong monsoonal climate.

1.3) Stratigraphy

The Castlegate Sandstone comprises the capping unit of the broadly progradational Mesaverde Group. In its proximal reaches it is typically subdivided into three informal units, the Lower Castlegate, the middle Castlegate, and the Bluecastle Tongue (Chan & Pfaff, 1991; Olsen et al., 1995; McLaurin & Steel, 2007), with the Lower Castlegate Sandstone being the focus of this study. The proximal Lower Castlegate is interpreted as bedload dominated low-sinuosity braided high-net-to-gross sheet-sand deposits (Olsen et al., 1995; McLaurin & Steel, 2007) sharply overlying the floodplane-rich fluvial deposits of the Blackhawk Formation. In the distal reaches, the Lower Castlegate is typically represented by moderate-sinuosity (Mitten et al., 2020) single-thread meandering fluvial channels nested in backshore muds, shoreface incising fluvially dominated channels, tidal dominated channels, and estuarine channels (Pattison, 2018). Coastal-plain deposits may contain dinosaur footprints (Yoshida, 2000), which are commonly associated with transgressive flooding surfaces (Lockley et al., 1992). These distal deposits of the Castlegate conformably overlie the shallow-marine deposits of the Desert Member, and are transgressed and overlain by the deep-marine Buck-tongue of the Mancos Shale (Fouch et al., 1983).

The Lower Castlegate Sandstone was deposited in a humid, sub-tropical environment (Miall, 1994) with paleocurrent directions oriented E-SE from the Sevier orogen in the West to the Western Interior Seaway to the East (Willis, 2000; Yoshida, 2000; McLaurin and Steel, 2007; Pattison, 2018). Based on detrital zircon U-Pb data, there are multiple observed headwater tributaries for the Castlegate fluvial system (Bartschi et al., 2018; Pettit et al, 2019). Castlegate deposits observed at the type-section and Joe's Valley Reservoir represent two distinct tributaries within the overall Castlegate system (Figure 2; Pettit et al.; 2019).

Evidence of the mixing of these tributaries appears by Tusher Canyon (Bartschi et al., 2018; Pettit et al, 2019), approximately 100 km down-dip from both the type-section and Joe's Valley Reservoir. The upper Blackhawk Formation and Lower Castegate at Joe's Valley show a distinct ca. 1430 Ma Midcontinent signature and a ca. 1700 and 1775 Ma Yavapai-Mazatzal signature, as well as an active coeval volcanic terrain supplying grains of Campanian age. The type-section shows less defined age peaks, wider distribution of zircon ages, lack zircon populations from the Cordilleran Arc, and only one Cretaceous-aged zircon observed in samples (Pettit et al, 2019). Deposits sampled at Tusher Canyon show a distinct mixture of zircons from these two source areas. Mixing of these tributary systems is backed up by grain-size data from Robinson and Slingerland (1998) and Petter (2010), who observed smaller grain sizes at the northern fluvial system at the Castlegate type-section and Sunnyside Canyons and larger grain sizes in the southern tributary at Joe's Valley. Grain size at Tusher Canyon is incompatible with a fluvial system solely sourced from the Castlegate Type-section (Petter, 2010). An abrupt shift in grain size, as well as mixing of zircon parent groups is indicative of mixing of the Northern and Southern tributary transects of the Castlegate fluvial system.

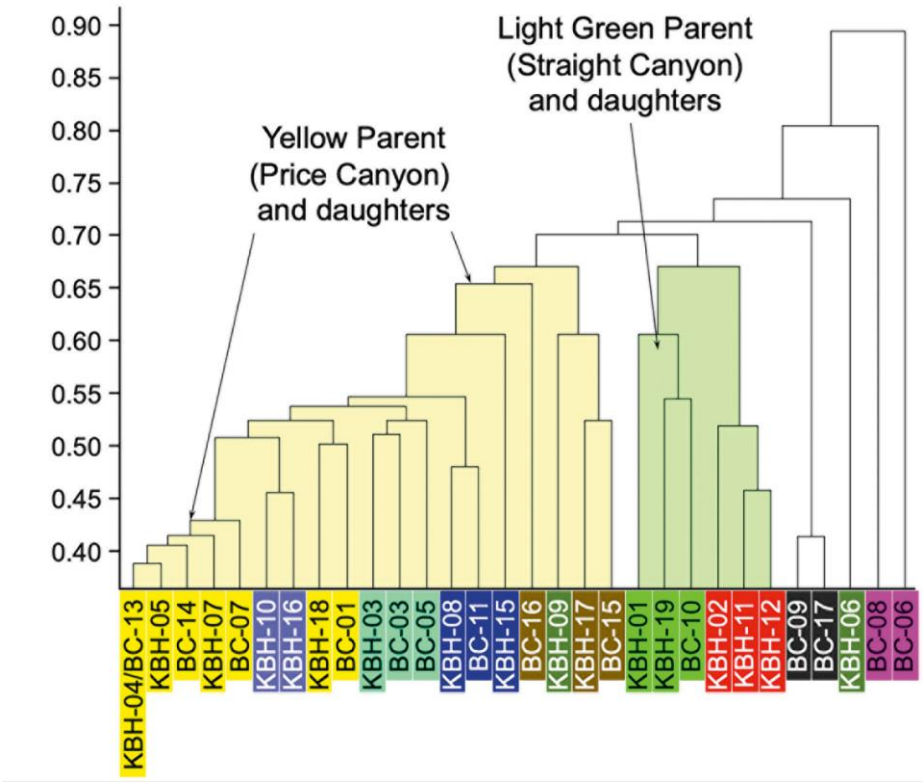

Figure 2: Dendrogram plot using cluster analysis based on U-Pb population characteristics showing distinct parent groups from Price Canyon (type-section) in yellow and Straight Canyon (Joe's Valley) in green. From Pettit et al. (2019).

The Lower Castlegate has historically been interpreted to be an incised valley fill bound by a regional basal scour representing a 3rd order sequence boundary either with or without a protracted hiatus (Van Wagoner et al. 1990; Van Wagoner 1991, 1995; Miall 1993, 1994, 2014, 2016; Yoshida et al. 1996, 1998; McLaurin & Steel 2000, 2007; Willis 2000; Yoshida 2000; Miall & Arush 2001a, 2001b; Hettinger & Kirschbaum 2002; Hampson 2010, 2016; Seymour & Fielding 2013; Hampson et al. 2014; Cross 2016). The formation of an incised valley of at least 80 km wide (Van Wagoner, 1995) is interpreted as the result of either eustatic sea-level drop (Van Wagoner, 1995) or tectonic controls and increased sediment supply (Miall 1994, 2001, 2014; Yoshida et al, 1996, 1999; Yoshida, 2000; Adams

& Bhattacharya, 2005), both of which imply a reduction in accommodation created in the system to generate the basal sequence boundary. Implications of applying the conventional incised valley sequence stratigraphic model to the Castlegate is the interpretation that the base of fluvial Castlegate Sandstones represents an extended period of time. This interpretation of this surface as a 3rd order sequence boundary implies the Castlegate Sandstone is separated temporally and genetically from the underlying Desert Member shoreface deposits (Van Wagoner, 1995).

Recent studies have questioned the incised valley model, and the existence of a through-going basal unconformity. These studies interpret the basal surface Castlegate Sandstone as a conformable contact throughout the proximal and distal reaches of the system (Hajek & Heller, 2012; Howell et al. 2018; Pattison, 2018, 2019 a, b, 2020; Pettit et al., 2019; Chamberlin & Hajek, 2019, 2022). Reinterpretation of the Lower Castlegate as lacking a basal unconformity is strongly supported by recent correlation to regional eustacy across the WIS (Howell et al., 2018) showing no large-scale eustatic drop in other regions of the WIS during deposition of the Castlegate. With lack of evidence of a regional eustatic sea-level drop, an incised valley created by a drop in sea-level is unlikely (Howell et al., 2018). This is supported by lack of change in provenance across the Blackhawk-Castlegate boundary in the proximal and distal reaches, with the same fluvial systems depositing both units, and the basal surface of the Castlegate Sandstone at the type-section incorporating very little time (Pettit et al., 2019; Sundell et al., 2024). The primarily low-angle ascending shoreface trajectories throughout the Desert Castlegate interval (Pattison, 2020) confirm that progradation of the system was not controlled by a drop in eustatic sea-level. The shoreface deposits of the Desert Member have been tracked up-dip, pinching out into near-shore muds,

with the backshore muds being trackable directly to Castlegate fluvial deposits, meaning that the Desert Member shorefaces were directly sourced from the Castlegate fluvial system (Pattison, 2019a, 2020). Analysis of shoreface-incising fluvial channels supports that these channels are typically directly related to the shoreface that they incise (Pattison, 2018). All of these studies support the Desert Member to Castlegate transition as a conformable sequence with the strongly progradational nature fed directly by river of the Castlegate Sandstone feeding sediment supply into the basin. These recent studies along with those showing no evidence of continuously traceable stratigraphic surfaces (Miall & Arush, 2001; Hajek & Heller, 2012; Pattison, 2018) and no change in fluvial style and channel size across the Blackhawk-Castlegate boundary (Adams & Bhattacharya, 2005) argue strongly that the shallow marine Desert Member and fluvial Castlegate Sandstone are temporally and genetically related (Pattison, 2018, 2019 a, b, 2020). Moving forward, the Desert Member and Castlegate Sandstone should be viewed as a conformable package with no evidence of incised valleys separating the fluvial and marine strata in time (Figure 3, Model C).

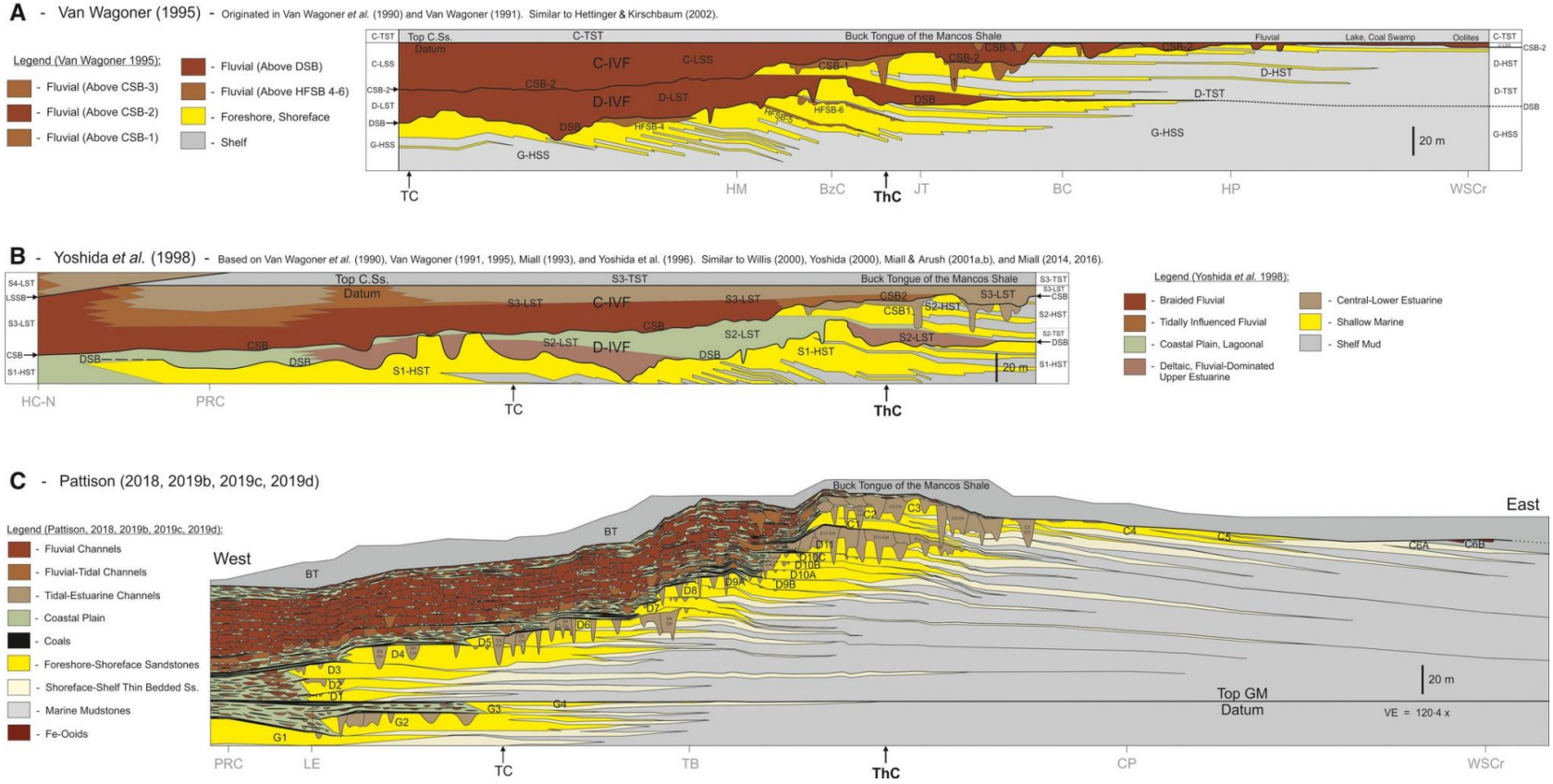
A - Van Wagoner (1995) - Originated in Van Wagoner et al. (1990) and Van Wagoner (1991). Similar to Hettinger & Kirschbaum (2002).
Legend (Van Wagoner 1995):
- Fluvial (Above CSB-3)
- Fluvial (Above CSB-2)
- Fluvial (Above CSB-1)
- Fluvial (Above DSB)
- Fluvial (Above HFSB 4-6)
- Foreshore, Shoreface
- Shelf
Top C.Ss. Datum
C-TST
C-IVF
C-LSS
CSB-2
D-IVF
D-LST
DSB
G-HSS
Buck Tongue of the Mancos Shale
CSB-1
CSB-3
HFSB-4
HFSB-5
HFSB-6
D-HST
D-TST
Fluvial
Lake, Coal Swamp
Oolites
20 m
TC
HM
BzC
ThC
JT
BC
HP
WSCr
B - Yoshida et al. (1998) - Based on Van Wagoner et al. (1990), Van Wagoner (1991, 1995), Miall (1993), and Yoshida et al. (1996). Similar to Willis (2000), Yoshida (2000), Miall & Arush (2001a,b), and Miall (2014, 2016).
S4-LST
LSSB
S3-LST
CSB
S1-HST
Top C.Ss. Datum
S3-TST
C-IVF
D-IVF
S2-LST
S1-HST
DSB
Buck Tongue of the Mancos Shale
CSB2
CSB1
S2-HST
20 m
HC-N
PRC
TC
ThC
Legend (Yoshida et al. 1998):
- Braided Fluvial
- Tidally Influenced Fluvial
- Coastal Plain, Lagoonal
- Deltaic, Fluvial-Dominated Upper Estuarine
- Central-Lower Estuarine
- Shallow Marine
- Shelf Mud
C - Pattison (2018, 2019b, 2019c, 2019d)
Legend (Pattison, 2018, 2019b, 2019c, 2019d):
- Fluvial Channels
- Fluvial-Tidal Channels
- Tidal-Estuarine Channels
- Coastal Plain
- Coals
- Foreshore-Shoreface Sandstones
- Shoreface-Shelf Thin Bedded Ss.
- Marine Mudstones
- Fe-Ooids
West
East
BT
Buck Tongue of the Mancos Shale
C1
C2
C3
C4
C5
C6A
C6B
D1
D2
D3
D4
D5
D6
D7
D8
D9A
D9B
D10A
D10B
D10C
D11
G1
G2
G3
G4
Top GM Datum
20 m
VE = 120·4 x
PRC
LE
TC
TB
ThC
CP
WSCr

Figure 3: Regional interpretations of the sequence stratigraphy of the upper Blackhawk and Castlegate Sandstone. Figures A and B represent the conventional sequence stratigraphic model of individual Castlegate and Desert Member IVFs with no tie between the Castlegate and underlying Blackhawk Formation. Figure C shows the new interpreted stratigraphic model tying the Castlegate Sandstone genetically and temporally to the Desert Member shoreface deposits with Castlegate fluvial strata directly feeding Desert Member marine strata (From Pattison, 2020). Model C is the preferred model for the Desert Member-Castlegate Sandstone interval. PRC- Woodside Canyon, TC- Tusher Canyon, ThC- Thompson Canyon.

Conventionally, studies have interpreted the Blackhawk-Castlegate transition in the proximal as a sequence boundary representing a substantial period of nondeposition or erosion (Van Wagoner et al. 1990; Van Wagoner 1991, 1995; Miall 1993, 1994, 2014, 2016; Yoshida et al. 1996, 1998; McLaurin & Steel 2000, 2007; Willis 2000; Yoshida 2000; Miall & Arush 2001a, 2001b; Hettinger & Kirschbaum 2002; Hampson 2010, 2016; Seymour & Fielding 2013; Hampson et al. 2014; Cross 2016). On the contrary, recent data supports the observation that the Castlegate basal scour is in fact an autogenically controlled basal scour resultant in increased sandy sediment supply to the basin (Hajek & Heller, 2012; Pattison, 2018, 2019, 2020; Chamberlin & Hajek, 2019, 2022; Pettit et al. 2019) representing very little missing time in the rock record (Pettit et al., 2019; Sundell et al., 2024). At multiple proximal and medial locations, the base of the amalgamated channel sands are observed interfingering with the underlying floodplain-rich Blackhawk Formation (Pattison, 2020). Recent evidence that there is very little erosion at the Castlegate type-section, with full-bar rollover observed throughout the section (Chamberlin & Hajek, 2019; Mitten et al. 2020) supports a high-accommodation system with no large incisional surface. The observed increase in coarser grains and reduction in fine-grained sediment provided into the basin over the Blackhawk-Castlegate boundary (Chamberlin & Hajek, 2022) may explain the sharp contact between the floodplain-prone Desert Member and overlying amalgamated sands of

the Castlegate Sandstone without inducing substantial incision. All scour surfaces reported at the Castlegate type section are consistent with that of either simple channel incision with the highest order surfaces observed being consistent with those formed during channel-belt avulsion (Hajek & Heller, 2012; Chamberlin & Hajek, 2019). Regional, local, and bedform-scale mudstone percentages show that there was a substantial reduction in mudstone from the Desert Member into the Castlegate (Chamberlin & Hajek, 2022), resulting in deposition of high-accommodation stacked fluvial sands with very little overbank fines overlying the floodplain-rich Blackhawk Formation. The Castlegate system retains high accommodation with observed full bar-form preservation, with ~66% of avulsion related bars being fully preserved (Hajek & Heller, 2012; Chamberlin & Hajek 2019) despite its sandy, amalgamated nature. This is supported by the relatively high calculated subsidence rate of 0.19 mm yr^{-1} and high ratio of bar top to erosional surface ratio of 2.5 at the type-section (Mitten et al. 2020). These high levels of barform preservation in the proximal are resultant of relatively high accommodation system (Mitten et al. 2020) as well as compensational river avulsion patterns (Chamberlin & Hajek, 2019).

Subsidence rates and barform preservation reduce substantially and abruptly West to East into the more distal reaches of the system, while channel sinuosity increases (Mitten et al. 2020). Subsidence curves were created using burial history based on thicknesses and lithologies observed from 10 boreholes down depositional dip (Mitten et al. 2020). Approximately 45 km East of the type-section at Sunnyside Canyon, subsidence rate has reduced to 0.11 mm yr^{-1} with an observed transition to more channel-form dominated architectures rather than the bar-dominated architectures observed up-dip (Mitten et al. 2020). Another 60 km Southeast at Tusher Canyon, subsidence rates have reduced further to

0.08 mm yr^{-1} and came with a much more sinuous fluvial system manifested by a substantial increase in lateral accretion elements and increased paleocurrent variability (Mitten et al., 2020). This change in architecture from proximal to more distal is typical for down-stream evolution of a fluvial system (Holbrook et al., 2006; Li et al., 2015; Mitten et al., 2020).

Figure 4: Blakey map of the KWIS in the Middle Campanian, 77.0 Ma. Utah outlined in black, approximate study area outlined in red.

CHAPTER TWO: Methods

The Castlegate Sandstone in the Book Cliffs is a world-class exposure of cliff-forming fluvial strata transitioning eastward into nearshore and marine sedimentary deposits (Van de Graaf, 1972). This exposure and longitudinal continuity permit a relatively well-connected outcrop belt from proximal-medial-distal reaches within the Castlegate fluvial system, and an opportunity to observe fluvial architecture and changes within fluvial strata down depositional dip. Outcrops were chosen along depositional dip to sample a well-linked updip to downdip transect for the Castlegate Sandstone using easily accessible outcrops where available. Outcrops were also chosen based on level of induration and visibility of architectural elements and sedimentary structures as well as lateral continuity of the outcrop. Nine total outcrops were utilized in this study (Table 1).

Outcrop	Name	Latitude	Longitude
1	Salina Canyon	38°53'54.52"N	111°30'59.83"W
2	Joe's Valley Reservoir	39°17'34.41"N	111°16'15.75"W
3	Type-Section	39°44'54.92"N	110°53'0.84"W
4	Sunnyside Canyon	39°34'2.76"N	110°22'27.55"W
5	Woodside Canyon	39°14'23.55"N	110°13'53.63"W
6	Crescent Canyon	39° 0'4.38"N	109°48'22.29"W
7	West Blaze Canyon	38°59'46.32"N	109°45'22.91"W
8	Thompson Canyon	39° 1'17.79"N	109°42'46.56"W
9	Sulfur Canyon	39°12'17.54"N	109°17'44.30"W

Table 1: Outcrops used in this study listed from proximal (1- 3) to medial (4-5) and distal (6-9). Measured sections and orthomosaics were collected for each outcrop.

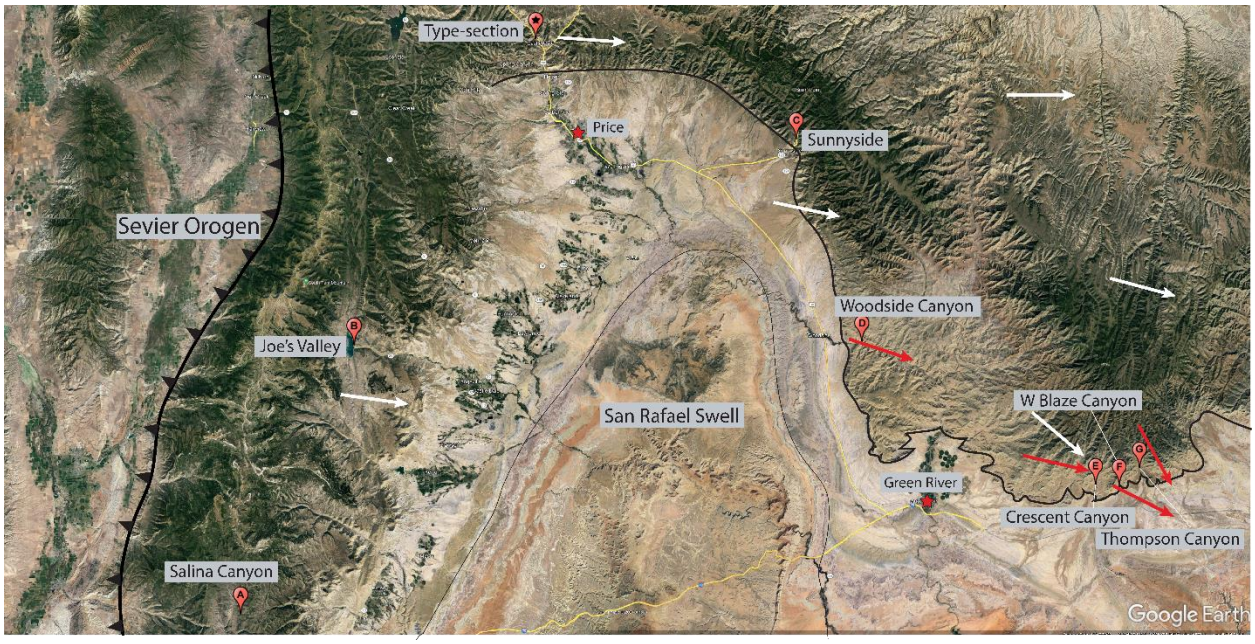

Figure 5: Outcrop locations labeled A-G. Black outline of the Book Cliffs outcrop. Locations of Price and Green River, UT labeled along with the modern location of the San Rafael Swell. White arrows are regional paleocurrent directions for the Castlegate (Miall, 2001), and red arrows are outcrop-specific paleocurrent averages (Pattison, 2018).

Methods used in this study are analysis of lithofacies, fluvial architectural element analysis, and the Fulcrum approach, as well as calculation of backwater length. Lithofacies were determined in the field at each outcrop studied through the collection of measured sections and mapped laterally onto finalized orthomosaics. Grain size, sorting, sedimentary structures, trace fossils, body fossils, and bar and channel architectures were recorded as lithofacies descriptors. Thicknesses were measured with tape measure, and when immeasurable, a Trimble Geo7x Range Finder was used from ground level. Where hand and Trimble measurements were not possible, large-scale features were measured in Agisoft using the generated 3D outcrop models. Measured sections were collected on-site at all

outcrops, excluding West Blaze Canyon due to inaccessibility of the outcrop. These measured sections were used to give localized facies ground truth, and lithofacies were then extrapolated laterally through the outcrop based on the visible architecture, color, and weathering properties of the observed facies.

A DJI Phantom 4 drone was used to obtain 3,752 detailed photographs across outcrop exposures, with photos containing substantial overlap to develop continuous orthophoto 3D models. These models were used for architectural element analysis and lithofacies correlations from measured sections. Photos were imported into Agisoft and processed using GPS data to align all photos, create depth maps to convert into a 3D outcrop model. These outcrop models were then flattened and converted into orthomosaic format to be used in figure generation. Finalized orthomosaics were then imported into Adobe Illustrator to be used to complete fluvial architecture analysis of the outcrops. Three-dimensional models and orthomosaics created in Agisoft are used to determine architectural elements and their hierarchical orders through tracking of bedding surfaces and lithofacies contrasts.

This study aims to use created orthomosaics to illustrate the fluvial architecture of the Castlegate Sandstone from its proximal to most distal reaches. Fluvial bounding surfaces were traced out on orthomosaics for each outcrop and assigned orders using methods outlined by Miall (1985, 1988, 1993, 1994, 1996) and Holbrook (2001). Surfaces were mapped on orthomosaics and assigned orders based on their hierarchy in outcrop, assuming lower order surfaces are bound by higher order surfaces, and surfaces can only be truncated by surfaces of similar or higher order (Holbrook, 2001). This hierarchy of fluvial bounding surfaces stretches from low-order bedforms and their bounding channel scours to the high-order surfaces such as valley and multi-valley scaled incisions that bound multiple channel

stories (Miall, 1985; Holbrook, 2001). Channel belts are observed as composite scours comprised by lower-order channel and bar scours, and valleys are determined by incision of 2 or more channel belts in thickness. The interactions of these surfaces and changes in fluvial style as well as incisional and aggradational patterns are used to determine the driving autogenic and allogenic factors causing variation in the observed architectures.

To determine backwater length, outcrops were analyzed using methods outlined by van Yperen et al. (2021). Backwater length (L_b) is calculated using average bankfull flow depth (h_m) and channel slope (S), using the equation (Paola & Mohrig, 1996):

$$L_b = \frac{h_b}{S}$$

Where backwater length is the distance before mean sea level intersects the depositional slope of the channel base. Both average bankfull depth and slope are calculated upstream of the backwater length at an area of normal flow (Trower et al., 2018).

Full channel stories were measured in outcrop where available to determine bankfull depth. This was done using barforms showing complete or partial rollover. When full-story barforms are not available, bedform sizes were measured, such as thickness of trough cross-beds or wavelength of cyclic steps to estimate the bank-full water depth of the channel. Cross-sets were preferentially measured near the base of a channel incisions in an attempt to capture the most accurate maximum flow-depth. Mean cross-set thickness was used to calculate mean dune height using the methods of Leclair and Bridge (2001), stating $h_m = 2.9(+0.7)\ S_m$ where h_m = mean dune height and S_m = mean cross-set thickness. Mean dune height (h_m) can then be used to calculate average channel flow depth (d_m) using the methods of Leclair and Bridge (2001) where $6 < d_m/h_m < 10$ and $d_{max} = 2d_m$.

Once full channel depth is known, it is possible to calculate channel slope using the empirical equation (Holbrook & Wanas, 2014; Trampush, Huzurbazar, & McElroy, 2014):

$$\tau^{*}_{bf50} = \frac{(h_m \cdot S)}{(P \cdot D_{50})}$$

Where τ^{*}_{bf50} is the Shields number for dimensionless shear stress, and is assumed to be 1.86 (Holbrook & Wanas, 2014). h_m is equivalent to d_m, and is average bankfull depth of a trunk channel. S is slope, and P is submerged sediment density, assumed to be 1.65 g/cm^3 for quartzose sandstone (MacKenzie & Poole, 1962; van Yperen, Line, et al., 2019). D_{50}, or median grainsize, values were sampled from normal channel-fill deposits lying directly above the thalweg deposits in representative trunk channels, resulting in analysis of the coarsest grains transported as bedload (van Yperen et al., 2021).

CHAPTER THREE: Results

3.1) Architecture

Salina Canyon:

Salina Canyon is the southernmost proximal outcrop in the study, and comprises ~53 m of fluvial sandstone sheets. The highest order surfaces observed in Salina Canyon are 6th order channel-belt scours. Grain size is typically quite homogenous so individual channel-bounding scours and other bounding surfaces are cryptic, with no barforms observed in the orthomosaic. Architectural elements observed in Salina Canyon are lower-flow sheet deposits, upper-flow regime sheet deposits, and overbank splay deposits. The basal sheets comprise only lower-flow regime deposits, with upper-flow regime bedforms increase in frequency up-section (Figure 7). The up-section shift in architecture coincides with an up-section increase in grain size observed in the outcrop. Overbank deposits in this outcrop are uncommon, with one substantial overbank lens observed.

Lower-flow channel fill facies range in thickness from 2.5-4 m thick, and are composed of medium-coarse grained sandstone dominated by trough to low angle cross-bedding. These deposits also locally show convoluted bedding. The base of channel sheets may contain small gravel lags at a channel thalweg. Between these sheets, thinly laminated, rippled, and local trough cross-laminated silt and fine sand splays may be preserved, though they are most commonly <30 cm in thickness.

Up-section, channel-belt sheets are observed with a substantial increase in flow regime including upper-flow regime chutes and pools, antidunes, and upper-plane beds as well as transitional bedforms (Figure 8). These deposits are bound by large, highly erosive

basal scours with local deeper, concave-up undulatory incisions. Deposits of the highest flow-regime are nested within these deeper undulatory scours and are likely coincident with the hydraulic jump created by these channel-bed lows. Bedforms interpreted as antidunes show the typical convex-up basal scour and are backfilled with coarse-pebbly sandstone (Figure 8).

Sand sheets containing upper-flow regime bedforms are typically bound at their base by highly undulatory scour surfaces with channel belt sheets reaching 6 m thick at the location of their deepest incision. These upper-flow deposits typically fine upwards from very coarse-pebbly sands at their base to lower coarse sands where channel tops are preserved, though they typically incise into the underlying sheet, so preservation of channel tops is rare. Sedimentary structures in these deposits show a decreasing flow regime upwards in a single sheet. At the basal incisions of the highest-flow regime channels, chutes and pools and antidunes are observed, which may transition upwards into planar beds. Other channel forms with flatter scour surfaces may show only planar bedding transitioning up-section into trough cross beds in an individual sheet (Figure 8). These deposits may contain convoluted bedding within channel fill deposits. Overbank deposits in this interval are preferentially removed due to the highly erosive nature of these upper-flow regime deposits, though locally thin overbank splay deposits are preserved. These overbank deposits may contain planar-bedded sands with gravel lenses, trough cross-laminated sands and silts, and rippled silts with minor carbonaceous matter on ripple and trough foresets.

Flow depth calculated for the best preserved antidunes in the outcrop indicate a paleoflow depth of ~2.21 m during deposition (Figure 8). Partially preserved antidune forms observed in outcrop indicate a minimum antidune wavelength of 7.6 m. Given antidune

wavelength, water depth can be determined using the equation $h_m = \lambda/2\pi$ where h_m is flow depth and λ is antidune wavelength. Given the estimation of minimum antidune wavelength, the minimum paleoflow depth can be calculated. The minimum paleoflow depth calculated for the antidune measured is 1.21 m. This antidune lies ~1 m from the base of the channel scour, so maximum channel depth can be estimated at 2.21 m.

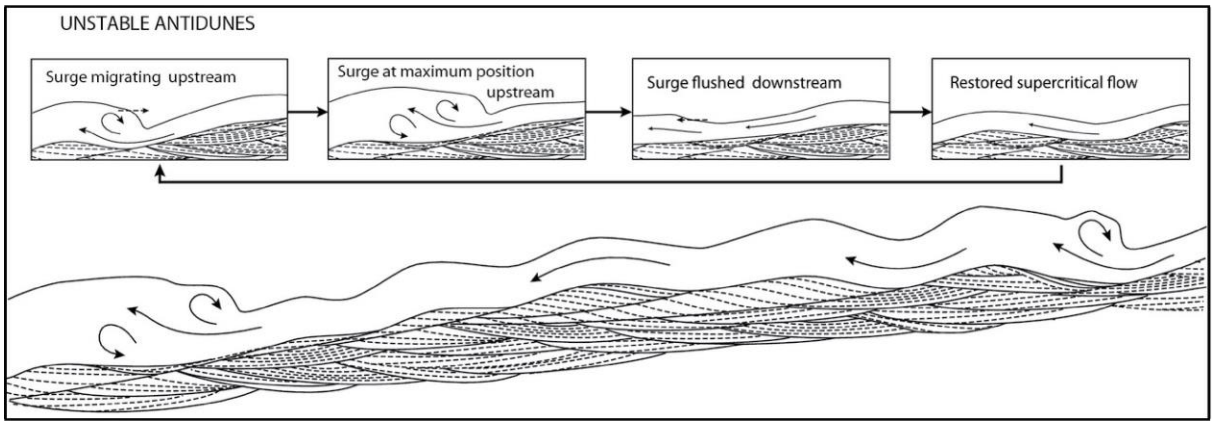

Figure 6: Unstable antidune bedforms similar to bedforms observed in Salina Canyon (Figure 8). From Cartigny et al. (2013)

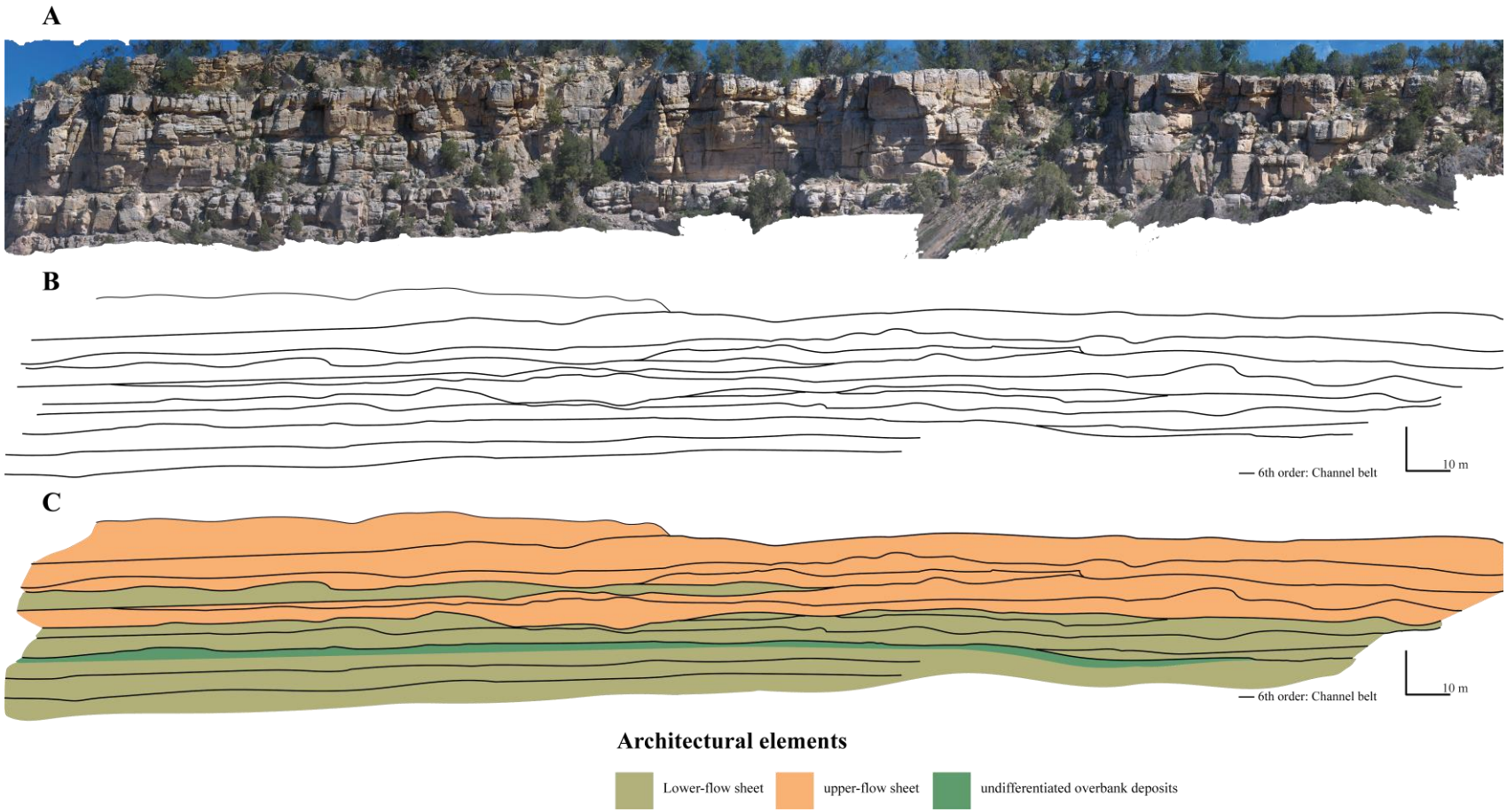
A
B
— 6th order: Channel belt
10 m
C
— 6th order: Channel belt
10 m
Architectural elements
Lower-flow sheet
upper-flow sheet
undifferentiated overbank deposits

Figure 7: Image of the outcrop studied (A), interpreted bounding surfaces (B), and bounding surfaces with color-coded architectural elements (C) for Salina Canyon.

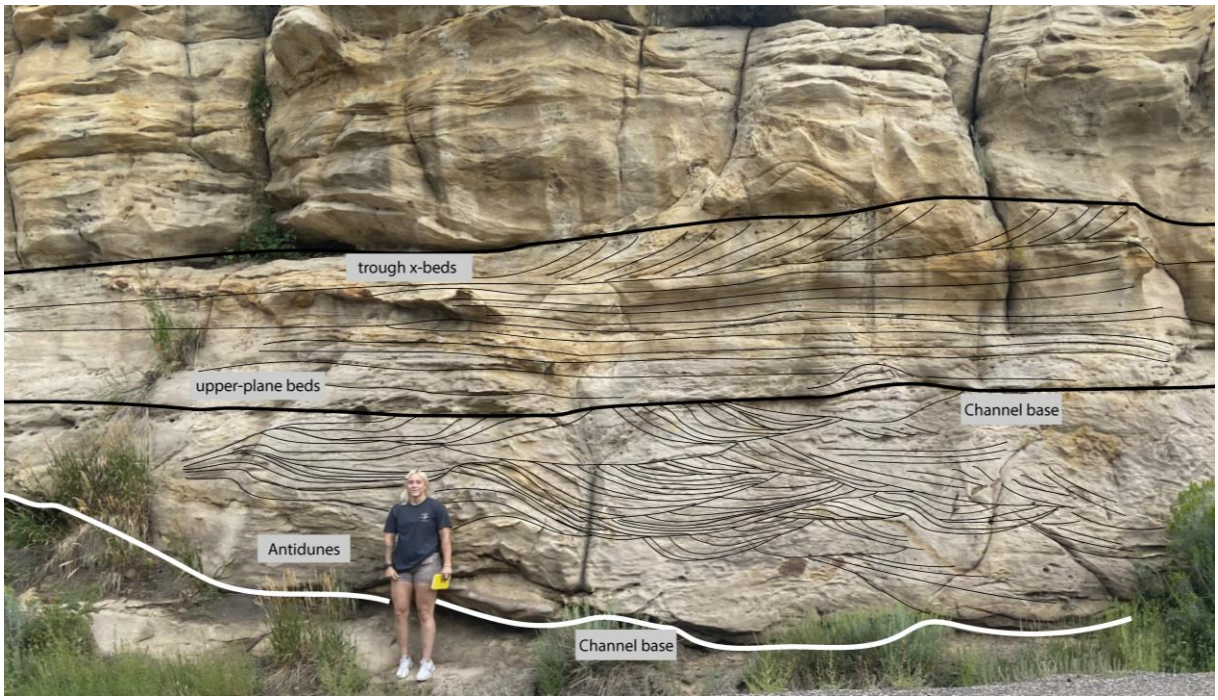

***Figure 8*:** Stacked flood sheet deposits in Salina Canyon. Basal sheet bound by a large scour, and filled with large antidunes with a minimum wavelength estimated at 7.6 m. Overlying this is another flood sheet with a less erosive base, filled with planar beds and local convoluted bedding transitioning up into trough cross-beds. Person 1.68 m for scale.

Interpretation

Outcrop at Salina Canyon shows an up-section increase in stream energy in the system, and a substantial increase in flooding events. Channels preserved in the upper section of Salina Canyon are indicative of upper-flow channels incised during maximum flood, and deposited under waning-flow conditions. The up-section occurrence of large upper-flow regime sheets is indicative of substantial flooding events where the channel is deeply scoured during waxing flow conditions, and transitions into an aggradational phase during waning flow, and generally create channel scours that are wide and sheet-like (Foley, 1977;

Alexander & Fielding, 1997; Froude et al., 2017; Slootman & Cartigny 2018; Wang & Plink-Björklund, 2019). There is likely lower-flow regime deposition occurring between flooding events, but the highly erosive nature of these upper flow regime sheets is not conducive to preservation of the normal-flow sediment that fill the channel belt prior to a flooding event. The large concave-up scours at the base of these channel sheets contain the highest flow regime deposits, and they likely represent the formation of chutes and pools resulting and resulting fill by antidunes due to hydraulic jump (Alexander et al., 2001; Lang & Winsemann, 2013; Cartigny et al., 2014; Slootman et al., 2019, 2021). The lack of these upper-flow regime bedforms in the lower interval of the outcrop and their dominance towards the top signifies an up-section increase in large-scale flooding events in the Castlegate system at Salina Canyon due to a shift in climate.

Joe's Valley Reservoir:

The Castlegate Sandstone at Joe's Valley reservoir comprises ~68 m of fluvial sand sheets and overbank splays. Architectural elements observed are valley-fills, channel belts, channel-fill, barforms, overbank splays, and heterolithic channel fill elements. Sandy channel belts and their nested channel-fill and downstream accreting barforms are the dominant architectural elements observed. Deposits at Joe's Valley fall into two intervals, which are separated by the first 7th order surface representing the first valley-fill and its equivalent terrace.

The highest order surfaces at Joe's Valley are 7th order valley-scale incisions with scour depths up to 10-12 m, and are filled with multi-story channel and barform elements. These surfaces occur only in the upper portion of the section, and coincide with increased preservation of overbank deposits on their respective terraces. 6th order surfaces contain

channel-belt deposits, which are typically one channel-story thick. These single-story channel-belts are the dominant elements observed in Joe's Valley. These channel belt deposits comprise 5th order channel and bar bounding surfaces, which in turn contain 4th order inter-channel and bar surfaces.

The lower interval of the Castlegate Sandstone at Joe's Valley Reservoir is dominated by highly amalgamated 6th order channel belt sheets. These sheets comprise channel-fill deposits and down-stream accreting barforms. Channel-fill is composed of trough cross-laminated upper medium-coarse sandstone with rippled caps where preserved. Rippled channel tops may have imprints of plant fragments on their surface. Individual channel forms may also contain a gravel thalweg at their base with gravels of a maximum diameter of ~1 cm. Channel-fill and barforms in this interval are typically more homogenous, and channel and bar bounding surfaces may be cryptic. Barforms observed with full or partial rollover indicate an average paleoflow depth of ~3.1 m with a maximum of 3.8 m and minimum of 2.5 m in this interval. Where preserved, intra-channel belt deposits are minor overbank splays of rippled silt and fine sands, though these are minor elements in this interval.

The architectural elements of the upper interval of the Castlegate Sandstone comprise sandy channel-fill, barforms, substantial overbank deposits, and local heterolithic channel-fill. Valleys in this interval are filled with multiple stories of channel and barform deposits. Channel-fill deposits and barforms are the dominant elements in this interval, and comprise upper-medium to coarse trough cross-laminated with localized convoluted bedded sands and log casts in channel bases. Locally conglomeratic barforms and channel fill (Figure 10) are observed in this interval, though they are rare. Conglomeratic channels are poorly sorted with gravel clasts of 2-12 cm in diameter. Rarely, conglomeratic bars locally preserve gravely

overbank splay deposits of up to 1 m, transported over the bar top into the interfluve, grading laterally into sandy-silty laminated beds. Barforms in the upper interval indicate an average paleoflow depth of 4.52 m with a minimum thickness of 3.1 and a maximum of 6.1 m. These barforms indicate a substantially larger flow-depth in this interval when compared to the average of 3.1 m the lower interval. Heterolithic channel fill elements are rare. These channel fills are observed nested in larger overbank lenses, and incise into underlying channel belts. Heterolithic channels are concentrically filled with interbedded layers of sand and muds.

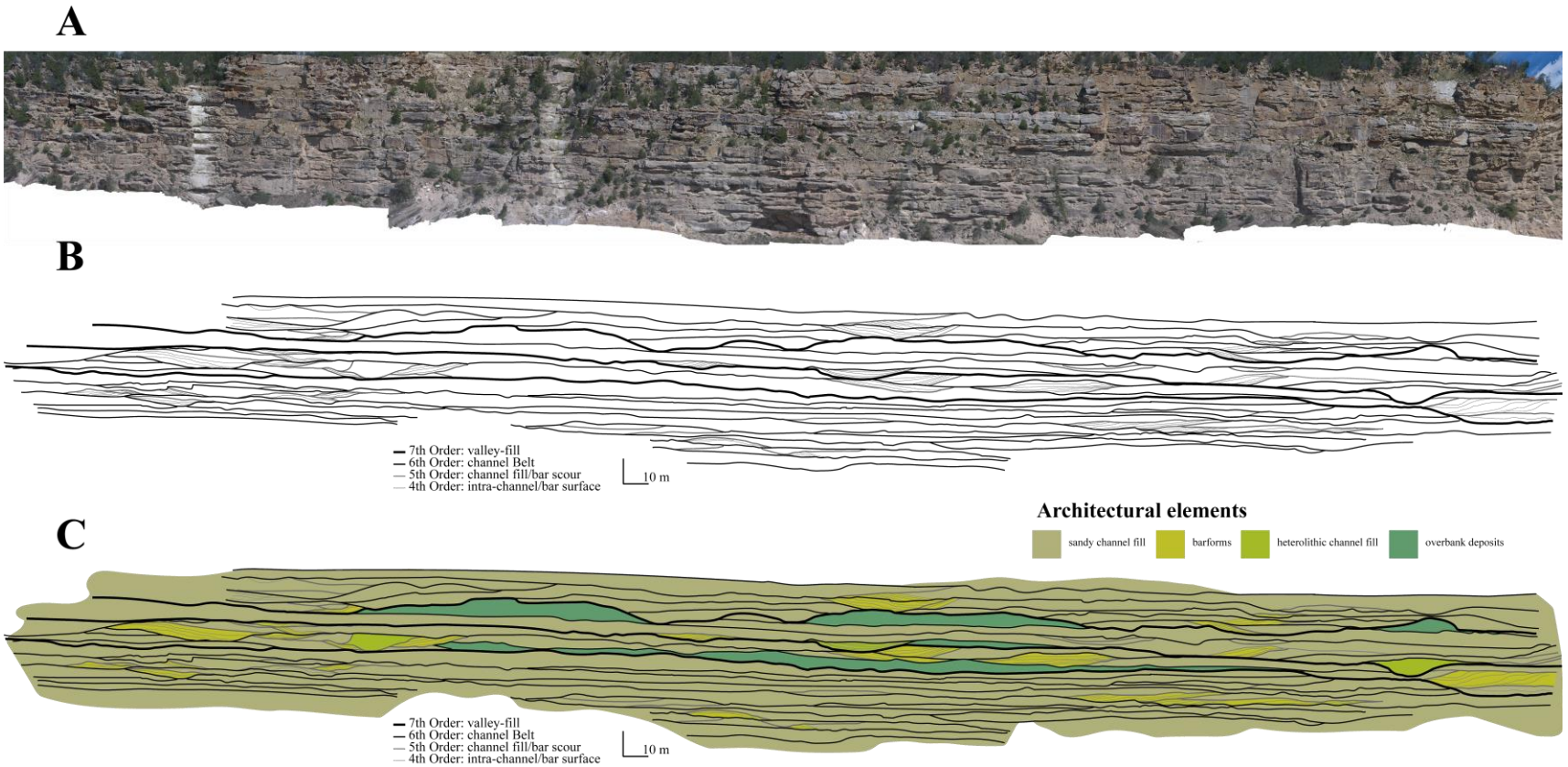
A
B
7th Order: valley-fill
6th Order: channel Belt
5th Order: channel fill/bar scour
4th Order: intra-channel/bar surface
10 m
Architectural elements
sandy channel fill
barforms
heterolithic channel fill
overbank deposits
C
7th Order: valley-fill
6th Order: channel Belt
5th Order: channel fill/bar scour
4th Order: intra-channel/bar surface
10 m

Figure 9: Image of the outcrop studied (A), interpreted bounding surfaces (B), and bounding surfaces with color-coded architectural elements (C) for Joe's Valley Reservoir.

Figure 10**:** Conglomeratic barform at Joe's Valley Reservoir with conglomeratic channel fill on the right of the photo. Gravels in bar are up to 12 cm in diameter.

Interpretation

The Castlegate Sandstone at Joe's Valley Reservoir records a shift up-section to deeper channels, increased incision, and increased overbank preservation. This pattern observed indicates an up-section increase in discharge and stream power within the Castlegate fluvial system. Increased paleo-depth observed up-section is indicative of an increase in discharge of the system.

Valley-scale incisions and increased average channel depth observed at Joe's Valley directly coincide with an increase in preservation of overbank muds on the terraces of valley

incisions. Previous studies at the Castlegate type-section have determined that an increase in channel-depth will result in increased scour spacing of fluvial channel deposits, and therefore increase overbank preservation (Hajek & Heller, 2012). This is consistent with the observed increase in flow depth recorded at Joe's Valley reservoir, where the lower, highly amalgamated and mudstone-poor interval has an average flow depth of 3.1 m, and the overlying strata showing increased mudstone preservation have an average flow depth of 4.52 m. It is apparent that overbank muds at Joe's Valley are typically observed preserved laterally on the terraces of localized valley-scale incisions. This is likely due to the increased confinement of the channel system during aggradation within a valley, resulting in reduced erosion of overbank facies laterally.

Valleys observed at Joe's Valley likely coincide with flooding events resulting in increased incision. These valleys do not coincide with larger sequence boundaries, thus are likely not representative of tectonic uplift. Valleys are observed locally along a surface, and are not seen nucleating from a specific surface on the outcrop. These valleys are simple cut-and-fill incisions that likely record singular events, and there is no record of increase in average grain-size up-section. The rare, localized nature of conglomeratic channels and bars are likely indicative of flooding events where river discharge increased substantially, allowing for the downstream migration of large gravel-sized clasts which are deposited as flow wanes, and their local nature is indicative of these high-flow periods representing a short amount of time. Localized evidence up-section of convoluted bedding is indicative of rapid deposition, which likely coincide with flooding events and subsequent deposition during waning-flow conditions.

Castlegate type-section:

The Castlegate Sandstone at its type-section comprises ~75 m of fluvial sands with two distinct intervals transitioning from highly-amalgamated channel belts at the base to larger, sheety channel belts with interbedded overbank lenses up-section. Channel belt deposits at the Castlegate type-section are dominated by channel fill and downstream accreting barforms. The highest order surfaces observed at the type-section are 6th order surfaces representing the base of individual channel belts. Internal to these channel belt sheets, 5th order channel scours and 4th order intra-channel and bar surfaces have been recorded. Overall, the Castlegate type-section shows an increase in fine-grained sediment when compared to the Southern proximal outcrops.

The lower portion of the Castlegate Sandstone is composed of amalgamated channel-belt deposits made up of channel fill and bar forms. These channel-belt boundaries can often be cryptic due to the highly amalgamated nature of these deposits. Channel fill is primarily composed of medium-grained trough cross-laminated sand with local examples of convoluted bedding. Channel thalweg deposits may contain small gravel lags. Bar forms are typically down-stream accretion elements and are composed of medium-grained sandstone that fine upwards. Barforms with complete or partial rollover record an average flow depth of ~3.04 m in this interval with a maximum thickness of 3.8 m and a minimum of 2.5 m. Overbank deposits in this interval lie between channel-belt deposits and individual channel forms are where preserved. Overbank deposits are thin with a maximum observed thickness of 30 cm in this interval.

The upper portion of the lower Castlegate at the type-section is composed of similar architectural elements to the lower, though there is an increase in overbank deposits and

channel-belt spacing. Channel forms in this interval are composed of trough cross-laminated to convoluted bedded medium-grained sandstone, with larger scale convoluted bedding observed in this interval. Downstream accretion barforms are composed of similar grain size to the lower portion of the outcrop, but locally show more interbedded fines between bar surfaces. Bars in this interval record an average paleoflow depth of ~4.41 m with a maximum recorded thickness of 5.1 m and a minimum of 3.7 m. These barforms show a substantial deepening of channels up-section at the Castlegate type-section, transitioning from an average of 3.04 m at the base to 4.41 m in the upper portion of the outcrop. This transition to larger barforms lies directly above the surface coinciding with the first substantial overbank deposit observed. Overbank deposits in this interval show an increase in carbonaceous material when compared to the lower interval, and consist of laminated to rippled splay deposits and distal interfluve carbonaceous muds and silts. Overbank muds are incised by overlying channel scours, resulting in discontinuous overbank lenses bound by channel-belt scours.

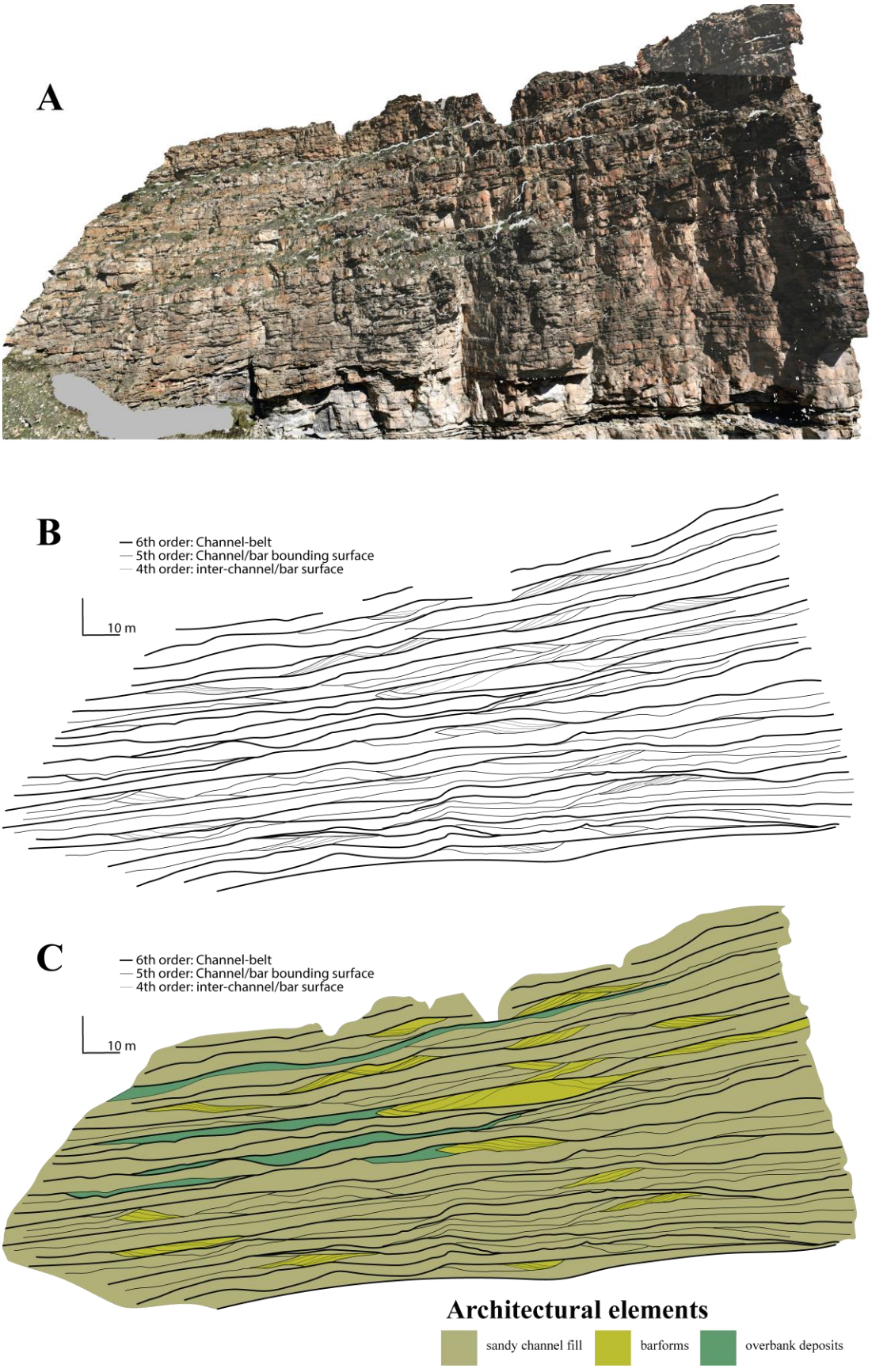
A
B
6th order: Channel-belt
5th order: Channel/bar bounding surface
4th order: inter-channel/bar surface
10 m
C
6th order: Channel-belt
5th order: Channel/bar bounding surface
4th order: inter-channel/bar surface
10 m
Architectural elements
sandy channel fill
barforms
overbank deposits

Figure 11: Image of the outcrop studied (A), interpreted bounding surfaces (B), and bounding surfaces with color-coded architectural elements (C) for the Castlegate type-section. (Image modified from VOG Group; Castlegate, VOG Group, https://v3geo.com/model/86)

Interpretation

The Castlegate type-section, similar to Joe's Valley Reservoir, shows an apparent channel deepening up-section coincident with increased mudstone preservation. Data collected in this study estimate a shift from 3.04 m in the lower sandy amalgamated interval, and 4.41 m in the upper Castlegate interval. This is consistent with previous studies with a recorded increase in flow depth from 2.6 m to 4.8 m (Hajek & Heller, 2012; Chamberlin & Hajek, 2019). The increase in mudstone in this interval is attributed to increased scour spacing due to increase in channel size (Hajek & Heller, 2012).

Increase in channel depth has been attributed to shift in climate, or an increase in fine-grained sediment supply or vegetation resulting in stabilization of channel banks (Hajek & Heller, 2012). There is no observed decrease in channel-belt width in this interval, and many barforms in this interval are incised into and nested in underlying channel sands, and still have increased barform thickness when compared to the lower interval. If overbank mudstones and vegetation were resulting in channel deepening, channel belts incising into other sandy strata would be expected to exhibit a reduction in flow depth, though they do not. Rooting of bar and channel tops is not recorded at this location, so it is not likely that vegetation was an influencing factor. An observed up-section increase in coaly material included in splay deposits is also recorded in the section measured suggesting distal overbank strata are deposited in an increasingly wet environment. Increase in coaly material up-section along with the increase in channel depth suggests a wetter environment for deposition of the

upper-section of the Castlegate. The Castlegate type-section is likely showing an increase in flow-depth due to climatic shift to a more wet environment and increase in monsoonal strength.

Sunnyside Canyon:

The Castlegate at Sunnyside Canyon comprises ~55 m of fluvial channel deposits. These deposits can be split into two intervals, with the basal portion composed primarily of large-scale amalgamated channel-belt deposits, and the upper dominated by ribbony distributary channels and an increase in overbank deposits. The highest order surface at this location is 6th order channel-belt scour surfaces. 5th order channel scour surfaces and 4th order intra-channel and bar surfaces have also been recorded. Due to the heterogeneous nature of the upper section, much of the exposure is covered, resulting in reduction of detail in observation of architectural elements. This outcrop lies on private property, so a partial measured section of the upper interval of the Castlegate was recorded where the outcrop meets the road.

The lower portion of the Castlegate sandstone is comprised by channel belts composed of large trunk channel deposits and barforms interpreted as downstream accretion elements. These channel forms are highly amalgamated, with bar rollover preserved locally. Barforms in this outcrop are often sandy, with localized thin fine-grained deposits interbedded with the inclined sandy strata. Barforms showing full or partial rollover in the lower interval record an average paleoflow depth of 5.03 m with a maximum thickness of 5.2 m and a minimum of 4.8 m, and show very little variation in thickness. Overbank preservation in this interval is low, with no substantial overbank deposits observed.

Overlying the lower amalgamated sandy unit is a typically ribbony, mud rich interval of the Castlegate with localized larger channel form elements. The measured section in this interval records small channels of ~1-3 m with interbedded fines. Channel forms in this interval are observed containing trough cross-laminated to rippled upper-fine to medium grained sands. Bases of channels and barforms in this interval contain rip-up clasts from the underlying overbank deposits. Overbank deposits typically consist of wavy-bedded muddy siltstone to fine sands with carbonaceous laminae. Overbank deposits in this interval are preferentially preserved within these ribonny fluvial deposits. No large trunk channels were present in the section measured, though they are observed locally in the orthomosaic.

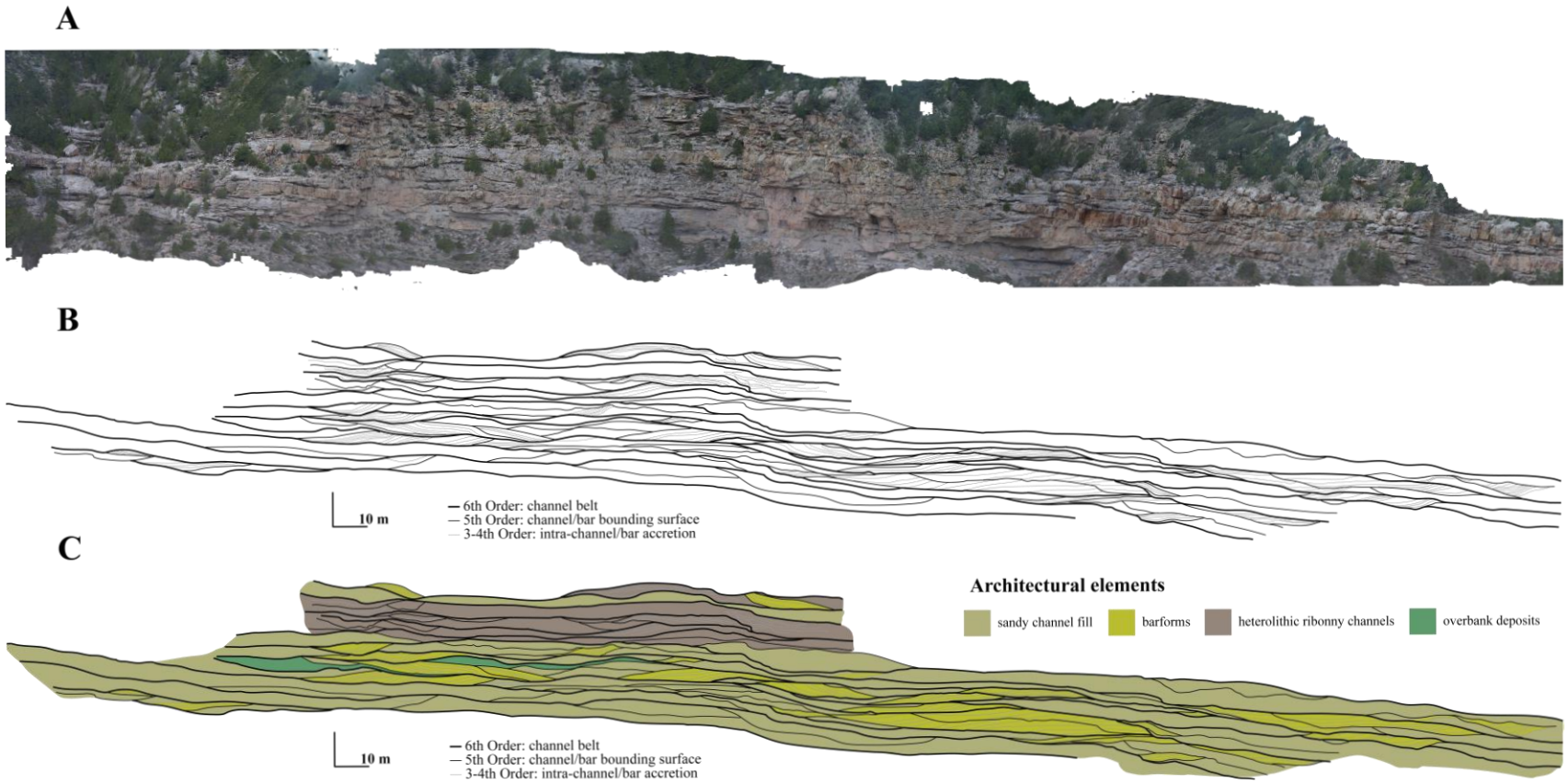
A
B
10 m
6th Order: channel belt
5th Order: channel/bar bounding surface
3-4th Order: intra-channel/bar accretion
C
10 m
6th Order: channel belt
5th Order: channel/bar bounding surface
3-4th Order: intra-channel/bar accretion
Architectural elements
sandy channel fill
barforms
heterolithic ribonny channels
overbank deposits

Figure 12: Image of the outcrop studied (A), interpreted bounding surfaces (B), and bounding surfaces with color-coded architectural elements (C) for Sunnyside Canyon.

Interpretation

The Castlegate Sandstone at Sunnyside Canyon has two distinct intervals. The first of which is large-scale channel forms and downstream accretion bars. The prevalence of downstream accretion bars in this location implies that the Castlegate at this location still shows a primarily braided fluvial style. The individual channel forms observed at this location are much larger than those more proximal and bars give an average estimated bankfull depth of 5.03. Bars used in this calculation only show partial rollover, so this is a conservative estimate of paleoflow depth, with other studies calculating paleoflow depths of 6.7 m based on cross-bed thickness (Mitten et al., 2020). This downstream increase in flow-depth can be attributed to the channels becoming increasingly single-thread down-dip coincident with the downstream evolution of the Castlegate fluvial system (Holbrook et al., 2006; Li et al., 2015; Mitten et al., 2020).

The upper interval at Sunnyside Canyon is composed primarily of small ribbony distributary channels nested in overbank deposits. Trunk channel deposits are observed locally in vertical section. These ribbony deposits are likely indicative of fluvial strata off-axis from the active channel belt, resulting in only minor distributary channels and overbank deposits. The prevalence of these smaller channel deposits likely indicates a large-scale migration of the main channel belt that fed the lower interval at Sunnyside Canyon. It is difficult to determine this for certain, as the outcrop is heavily covered due to the heterolithic nature of these deposits.

Woodside Canyon:

The Castlegate Sandstone at Woodside Canyon show a distinct shift in large-scale fluvial architecture from the more proximal outcrops in this study. Channel-belt deposits are the dominant architectural elements, and comprise channel-fill and barform elements. Multiple large-scale 7th order valley scale scour and fill events from 12-20 m in thickness and up to 1.2 km wide are recorded incising into channel-belt deposits. Valleys are observed cutting through multiple channel belts, and sandy valleys are filled with multiple channel stories. These valleys are observed filled with lacustrine deltaics, channel-belt deposits, and mudstones. 6th order channel belts, 5th order channel scours, and 4th order bar surfaces are recorded where apparent. A measured section for Woodside Canyon was collected further down the valley past where the dirt road crosses the Price River.

The observed architectural elements at Woodside Canyon are channel fill, downstream accreting barforms, lacustrine deltaics with distributary channels, heterolithic channel fill, overbank deposits, and undifferentiated mudstone filled valleys. Channel fill elements are typically trough cross-laminated lower-upper medium grained sands with local convoluted bedding. Barforms are medium grained sands, with an up-section increase in fines preserved between bar surfaces. When rollover is preserved, these bars record an average paleoflow depth of 5.5 m with an apparent increase in flow-depth up-section. Lacustrine deltaics are observed in one location, composed of interbedded inclined layers of muds and sands with prevalent carbonaceous and coaly layers. These deposits fill the largest valley scour observed in the area at ~20 m thick. Distributary channels are observed on the top of inclined strata, and increase in occurrence up-section. Heterolithic channel fill elements are composed of horizontal interbedded sands and coaly muds, and occur locally in

the upper portion of the outcrop. Overbank deposits in the lower portion of the outcrop consist of grey silts between channel fill elements and channel belts typically <50 cm thick, the thickest being ~1.5 m thick. Up-section, overbank deposits become increasingly carbonaceous and finer-grained. Overbank deposits recorded near the top of the outcrop may be silty with laminated muds and coaly material, or carbonaceous distal overbank mudstones.

The largest scour observed in this interval is 20 m deep valley fill that cuts out nearly all of the lower half of the Castlegate amalgamated sands. The base of this valley fill contains 5-6 m of single-story channel-fill elements. These channel fill elements are directly overlain by lacustrine deltaic strata. Lacustrine deltaic strata are comprised of inclined heterolithic beds of carbonaceous mud and coals and thinly bedded sandstone. These inclined heterolithic strata lap out onto the top of the channel fill element observed at the base of the scour fill. To the left of Figure 11, these heterolithic deltaics pinch out, leaving only a thick succession of fluvial channel sands. The mud-filled valley is interpreted due to the presence of a large scour into the upper portion of the Castlegate Sandstone removing multiple channel-belt stories of ~16 m in total thickness. The muddy nature of this valley fill results in it being covered, though in the slope some thin sandy layers are observed protruding from the cover. It is possible that this valley is also filled with lacustrine strata, though it is unclear due to lack of exposure. Other valleys in the study area contain fill of multi-story stacked channel-belt deposits.

It is noted that at the bottom-left of the orthomosaic (Figure 13), fluvial channels nested in overbank deposits transition laterally into the amalgamated sands. The Castlegate is typically determined by the base of the amalgamated fluvial sands, though it is apparent that this surface interfingers with the underlying muddier fluvial strata laterally. This makes

determination of the base of the Castlegate at this location cryptic. Depending on where the base of the Castlegate is placed, deposits at Woodside Canyon are anywhere from ~45-55 m thick.

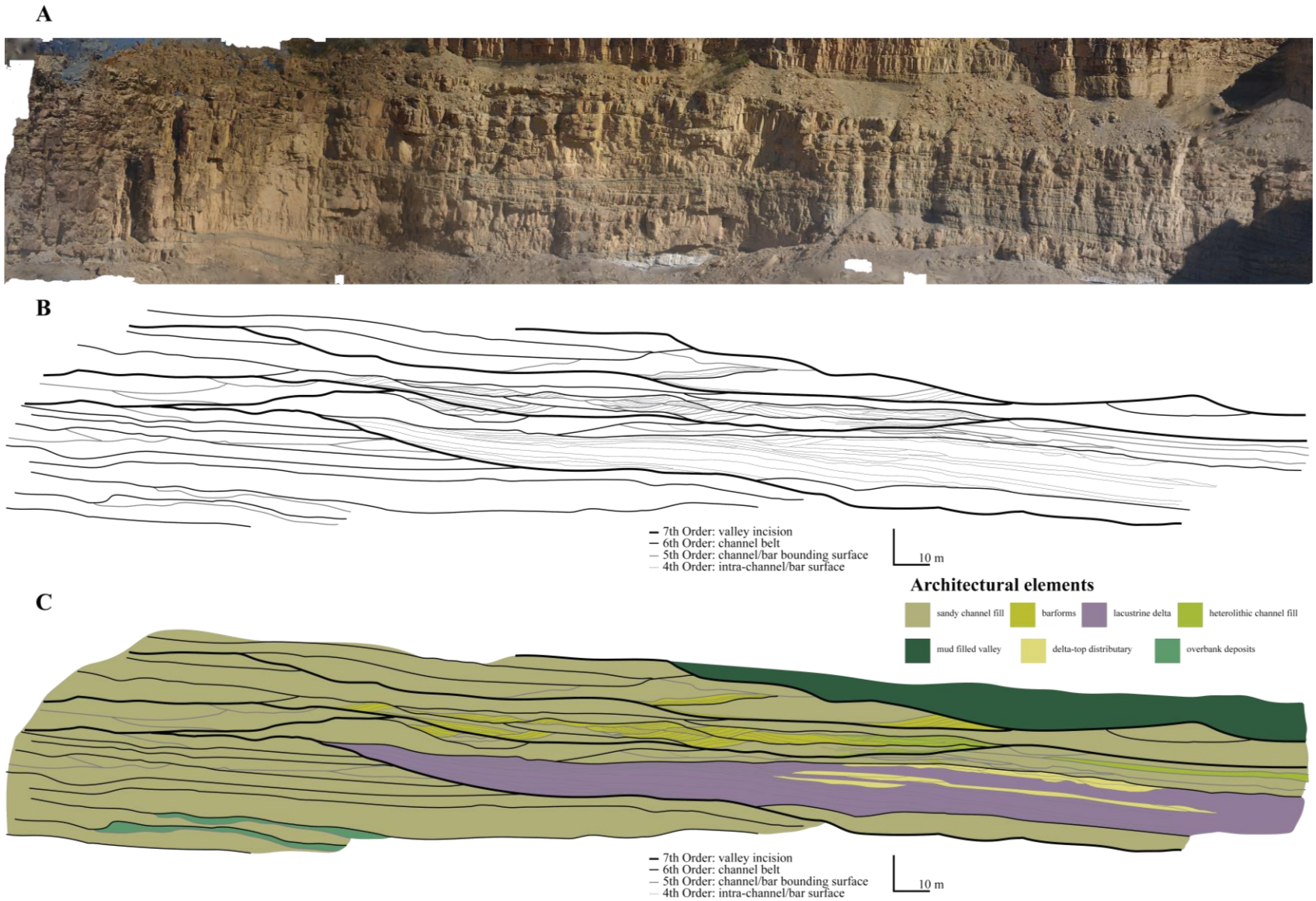
A
B
7th Order: valley incision
6th Order: channel belt
5th Order: channel/bar bounding surface
4th Order: intra-channel/bar surface
10 m
C
Architectural elements
sandy channel fill
barforms
lacustrine delta
heterolithic channel fill
mud filled valley
delta-top distributary
overbank deposits
7th Order: valley incision
6th Order: channel belt
5th Order: channel/bar bounding surface
4th Order: intra-channel/bar surface
10 m

Figure 13: Image of the outcrop studied (A), interpreted bounding surfaces (B), and bounding surfaces with color-coded architectural elements (C) for Woodside Canyon.

Interpretation

Woodside Canyon is observed with valley incisions representing periods of incision into underlying channel belts and subsequent filling. These valleys are isolated, and stacked vertically up-section and each represent individual periods of scour and subsequent aggradation with varying fill. Valleys of this scale are not observed up-dip nor down-dip from Woodside Canyon. The source of these valley-scale scours is discussed in depth later.

Valleys in this location are observed with varying fill types. The largest valleys recorded is filled at the base with a single-story channel-belt sheet, and subsequently filled with estuarine deltaic deposits. This represents abandonment of this incision after the basal tier of channel-fill. The valley was then subsequently filled with estuarine deltaics consisting of heterolithic inclined strata of sands, and carbonaceous muds and coaly layers, and delta-top distributary channels. Abandonment of this valley likely occurred rapidly during large-scale channel-belt avulsion up-stream leaving a nearly empty valley to be filled with lacustrine strata. The presence of lacustrine deposits and prevalent coals is likely indicative of a wet climate.

Other valleys are filled with multi-story channel-belt fill, and represent subsequent filling by the active channel-belt that cut the valley post-incision. The uppermost valley is interpreted as a mud-filled valley due to its recessed, covered nature. It is unknown what the fill of this valley is, though the lack of multi-story channel fill is indicative that the valley was abandoned by the active channel-belt before it was filled.

Crescent Canyon:

The Castlegate Sandstone at Crescent Canyon is an ~30 m thick fluvial deposit directly overlying a road-level coal layer. These deposits contain two distinct intervals, with the basal interval composed of nearshore meandering trunk channel and point bar deposits, and the upper interval is composed of a more proximal, single-story amalgamated sheet of channel sands. The highest order surfaces in this outcrop are 6th order channel belt surfaces bounding the bases of each distinct interval.

Architectural elements of the lower interval are sandy nearshore trunk-channel fill, point bar deposits, heterolithic channel fill, and overbank muds. The largest element observed is the large 19 m thick point bar with local complete rollover. This point bar shows complex internal architecture, with multiple growth periods bound by 5th order surfaces showing migration in a primarily S-SW orientation. This point bar is heterolithic, with inclined strata composed of interbedded fine-lower medium sands and silty muds. Sandy inclined strata contain ripples or inclined beds, and muds are rippled to massive. Bar tops are rippled fine sands with interbedded layers of lenticular muds and fine sands. Laterally this point bar transitions into a large nearshore trunk channel fill, which comprises lower-medium-grained trough cross-bedded sands. The base of the channel fill incises into the underlying nearshore muds, and contains large angular rip-up clasts. Incising into the top of this channel fill lies a heterolithic channel with interbedded fine sands and laminated-flaser bedded muds with inclusions of carbonaceous matter. Capping this lower interval is the overbank mud element, comprising massive, lenticular bedded to rippled mudstones with carbonaceous matter. Locally, thin rippled to trough cross-bedded sand sheets are observed nested in overbank muds.

Above the second 6th order surface lies a 7-13 m thick sheet of amalgamated channel sands. This sand lacks preservation of overbank deposits, and consists solely of sandy channel fill. This interval is dominated by trough cross-bedded lower medium sands. Internal bounding surfaces are cryptic due to the homogenous nature of this interval, though large single-story channel incisions can be seen cutting from the top of the sheet down to the base of the sand sheet. This fluvial sand sheet shows no evidence of marine influence nor tidal indicators. This is the most distal observed occurrence of such deposits in this study.

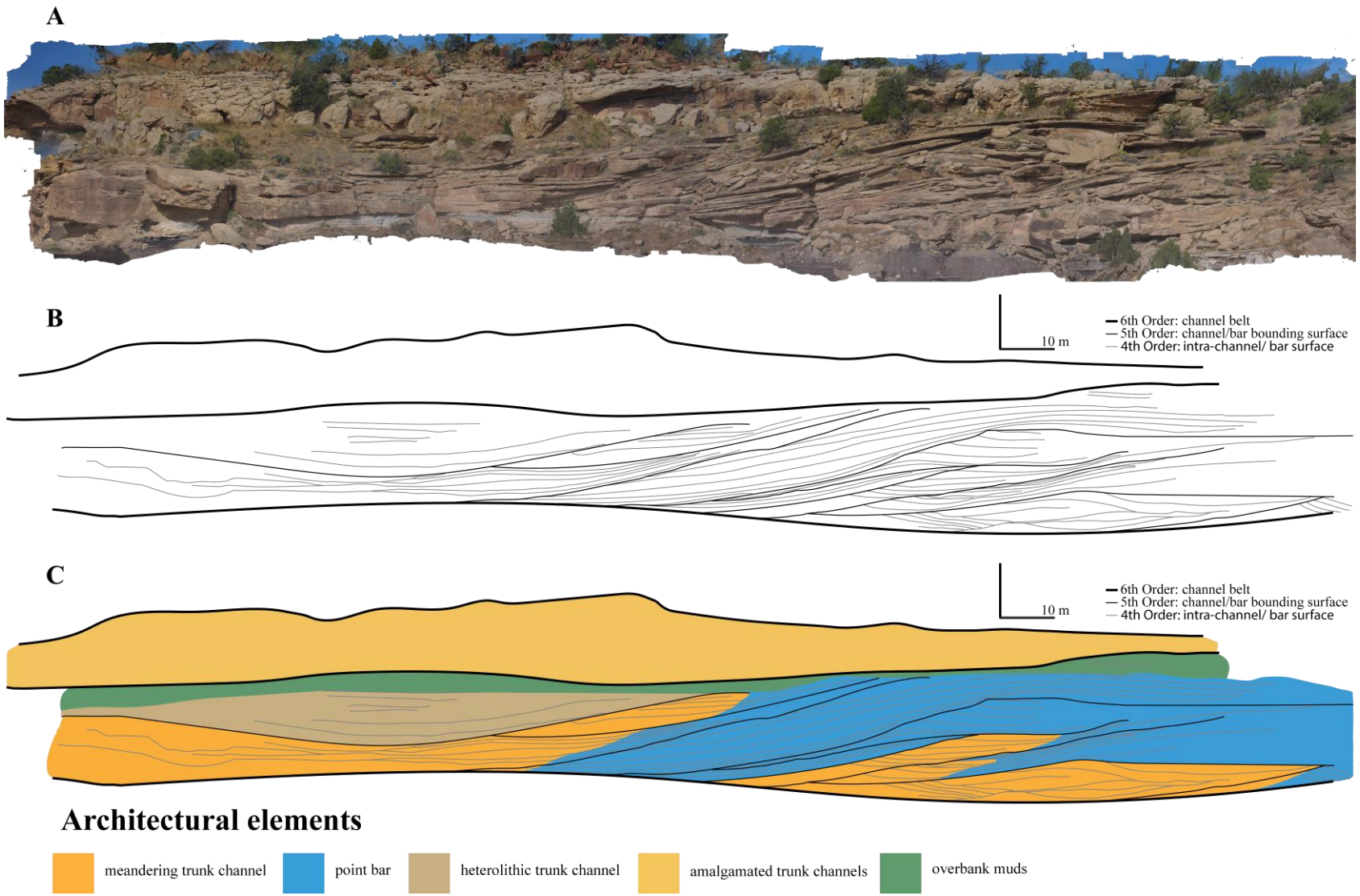
A
B
10 m
6th Order: channel belt
5th Order: channel/bar bounding surface
4th Order: intra-channel/ bar surface
C
10 m
6th Order: channel belt
5th Order: channel/bar bounding surface
4th Order: intra-channel/ bar surface
Architectural elements
meandering trunk channel
point bar
heterolithic trunk channel
amalgamated trunk channels
overbank muds

Figure 14: Image of the outcrop studied (A), interpreted bounding surfaces (B), and bounding surfaces with color-coded architectural elements (C) for Crescent Canyon.

Interpretation

The lower interval of Crescent Canyon is composed of large point bar and trunk channels. The full, single-story point bar indicates a paleoflow depth of 19 m based on bar thickness, which is the deepest channel observed in the study. This down-dip transition from sandy, amalgamated braided channels to sinuous, meandering channel-forms is consistent with the downstream evolution of a fluvial system (Holbrook et al., 2006; Li et al., 2015).

The prevalence of point bar deposits in this interval are indicative of relatively high sinuosity channel forms (Miall, 1994). The heterolithic nature of the point-bar deposits may be indicative that this channel is within backwater length and influenced by backwater hydrodynamics. Given the observed bankfull depth of 19 m and the system slope of 0.000199 m/km (Table 2), the backwater length for this river would extend for ~95 km. Crescent Canyon is within 60 km of the most basinward Castlegate shoreline (Figure 20; Pattison, 2020), therefore it must be within backwater reach. This river is a large, nearshore meandering fluvial system within one backwater length, nested in backshore muds. This is representative of a large tributary trunk channel chasing out the seaway as the system progrades. A modern analog for this trunk channel would be the Mississippi River near Baton Rouge, where large meandering point bar complexes are observed associated with a large, deep trunk channel (Rittenour et al., 2007).

Capping Crescent Canyon is the most basinward observable amalgamated, non-tidally influenced channel sandstone. These deposits record a shift to a more proximal fluvial style when compared to the underlying meandering fluvial deposits, consistent with the

progradation of the fluvial system. These are the most basinward channel deposits observed that lack marine influence. These deposits may represent low-accommodation, amalgamated trunk channel deposits feeding more distal Castlegate shoreface deposits, similar to those recorded in the Mesa Rica Sandstone of the Dakota Group (Holbrook, 2006; van Yperen et al., 2019). Due to the lack of evidence of tidal influence, these channels are outside of tidal reach, and it is possible that these deposits are outside of the backwater reach, though more evidence is needed to determine this. It is also possible that the transition from a meandering fluvial system nested in muds to amalgamated channel-sands may be controlled by change in river discharge, and sediment discharge of the system (Rittenour et al., 2007).

West Blaze Canyon:

West Blaze Canyon is represented by a ~4 m thick fluvial sheet with local valley-scale incisions of up to 16 m thick (Figure 15). These valley-scale incisions cut directly into the underlying marine Desert Member shoreface deposit, but are not observed incising below the base of the shoreface. A measured section was not collected at West Blaze Canyon due to inaccessibility. For this reason, only discussion of fluvial architectural elements is presented, with lithofacies inferred based on drone photographs and comparison to nearby outcrops containing similar lithofacies in measured sections.

The architectural elements observed in West Blaze Canyon consist of valleys filled with sandy shoreface-incising trunk channels, minor tidal channels, tidal lateral accretion sets, minor mouth bars, and sand and mud flats. These valley scours are bound by 6th order surfaces, and are filled with multiple stories of 5th order channel fill. The sandy shoreface incising channel (Large orange element, Figure 15) cuts from the top of the shoreface 10 m down to near the base of the shoreface. These deposits are nearly lithologically

indistinguishable from the surrounding shoreface besides their separation by a basal valley scour observed and reactivation surfaces representing multiple fill events with apparent trough cross bedding. Laterally within the valley scour, this transitions into heterolithic fluvio-tidal deposits consisting of channel-fill sands, mouth bars, and heterolithic lateral accretion sets. Lateral-accretion elements are heterolithic, and are interpreted based on inclined bedding and sigmoidal architecture. Mouth bars are indicated by concave down, sands forms with internal concave down 2-3rd order surfaces. Tidal channel fill is interpreted by trough cross bedded concave up sand lenses. The upper 6th order scour represents a nested valley with similar fill to the heterolithic fluvio-tidal deposits observed below, but with greater amounts of sand in the fill. This interval contains similar heterolithic tidal channel fill and lateral-accretion elements as well as mouth bar deposits. This upper valley fill incises into tidal sand flat and mud flat deposits. Tidal sand flats overlie the fluvial valley-fill. These deposits are interpreted as tidal flats due to interbedded ribbony sands and muds, which are visually identical to those observed at Thompson Canyon. Evidence of tidal influence in shoreface-incising channels is observed by Pattison (2019) with observation of double mud-drapes, *Teredolites* burrows, herringbone cross-bedding, and shell lag deposits.

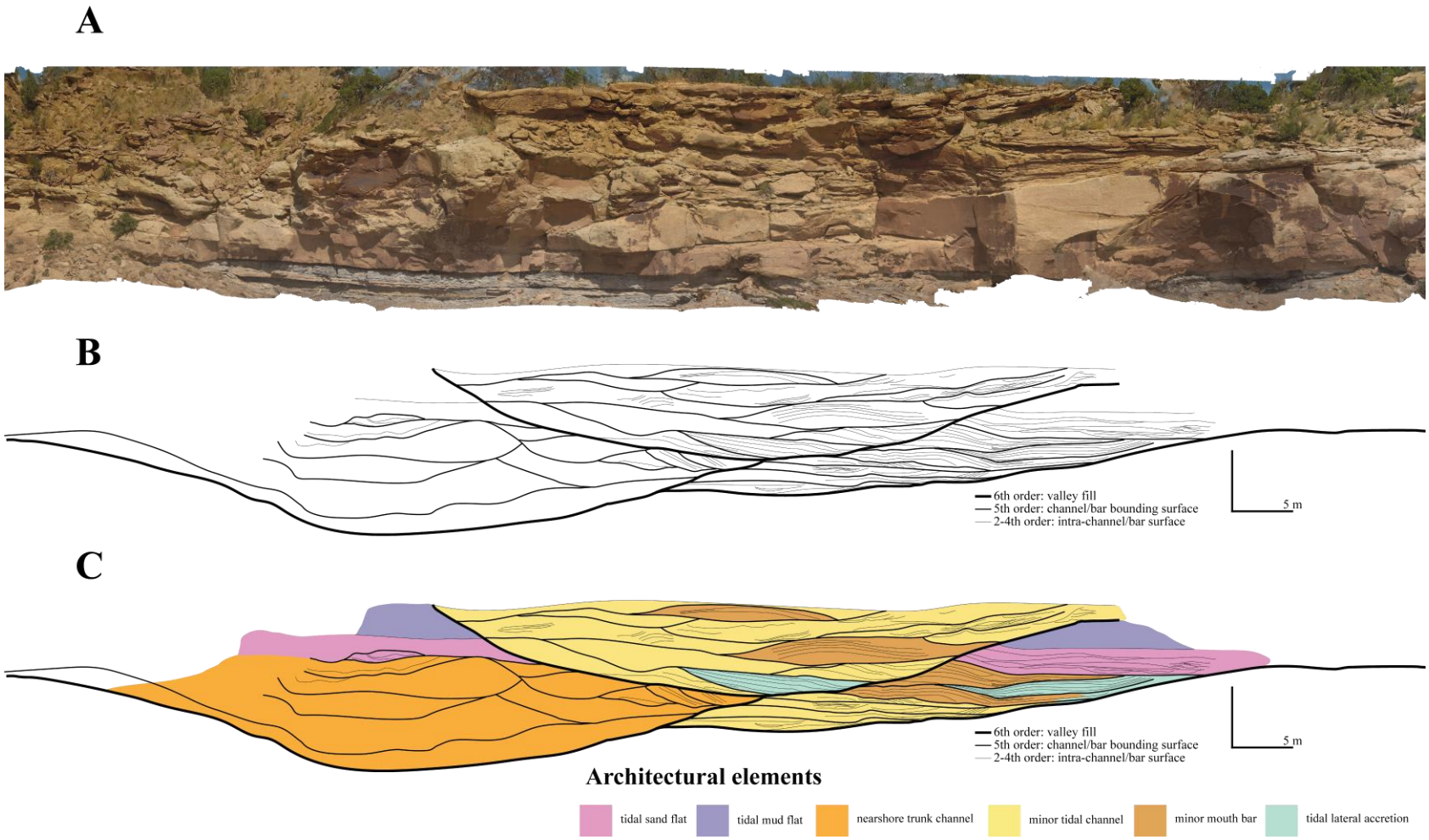
A
B
6th order: valley fill
5th order: channel/bar bounding surface
2-4th order: intra-channel/bar surface
5 m
C
6th order: valley fill
5th order: channel/bar bounding surface
2-4th order: intra-channel/bar surface
5 m
Architectural elements
tidal sand flat
tidal mud flat
nearshore trunk channel
minor tidal channel
minor mouth bar
tidal lateral accretion

Figure 15: Image of the outcrop studied (A), interpreted bounding surfaces (B), and bounding surfaces with color-coded architectural elements (C) for West Blaze Canyon.

Interpretation

The valleys observed at West Blaze Canyon are likely autogenic in nature (Trower et al., 2018; Pattison, 2019), and caused by flooding events inducing increased scour depths (Trower et al., 2018). The fact that these valley-fills show tidal influence leads to the interpretation that these valleys are within tidal range, and heavily influenced by tides. Data collected within distal deposits of the Castlegate Sandstone shows that flooding events can induce scour of up to 3x normal flow depth due to drawdown of the water surface to that of sea-level (Trower et al., 2018). Data presented in Trower et al. (2018) interprets all valley-scale incisions in the distal Castlegate strata as autogenically induced by backwater hydrodynamics.

Valleys observed in this interval are likely incised and deposited as distributary channels as the Castlegate channels reach strong tidal influence. These valleys and channel forms observed are much smaller than the trunk channel observed at Crescent Canyon, and likely represent the bifurcation and spreading of the fluvial system due to strong backwater influence. Previous studied have interpreted many of these distal shoreface-incising channels as distributary in nature (Pattison, 2018; Pettit et al., 2018).

Thompson Canyon:

The outcrop studied in Thompson Canyon lies above the uppermost shoreface deposit, and comprises at least 20 m of tidal and estuarine fluvio-deltaic deposits comprising delta clinoforms, mouth bar deposits, delta top distributaries and their lateral accretion bars,

trunk distributaries, and tidal mud and sand flats. The highest order surfaces observed are 6th order surfaces consistent with channel-belt avulsion.

At the base of the outcrop are inclined heterolithic strata of a minimum 9m thick, with the true base not visible owing to modern cover at the thickest portion. It is composed of trough cross-bedded to rippled fine-med sands of 20cm-1.5m and interbedded silts and muds with a maximum thickness of 20cm. The sand sheets contain climbing ripples, and rip-up clasts from their underlying finer counterparts. This interval has local *Teredolites* observed on basal surfaces of sand sheets.

A mouth-bar complex overlies the heterolithic inclined strata, and cuts into and bevels off the tops of the inclined strata. This is observed at the first 6^{th} order surface. These mouth bars consist of upper-fine massive to trough cross-bedded sands with localized *Teredolites* observed at their basal scours. Laterally, these are incised by heterolithic fluvial channel-fill deposits of trough-cross bedded to rippled fine sands and flaser-lenticular mud and sand. The channels in this interval contain heterolithic lateral-accretion elements composed of rippled fine sands and wavy laminated muds and silts.

Above this lies high width-to-thickness, laterally stepping and aggrading channels bound by a basal 6^{th} order surface. This interval is one channel-story thick, and records fine-grained sandstone channels with very little incision, simply lateral migration of channel-forms. These channels consist of fine-grained trough cross-beds with rippled intervals internal to an individual channel sheet. Above these laterally migrating channels lies ~2m of mud and sand flats, locally showing flaser-lenticular bedding, bidirectionally rippled ribbony fine-grained sands interbedded with flaser-lenticular bedded muds. Within these tidal flat

deposits minor vertical and horizontal *Skolithos* burrows are observed in localized sand sheets.

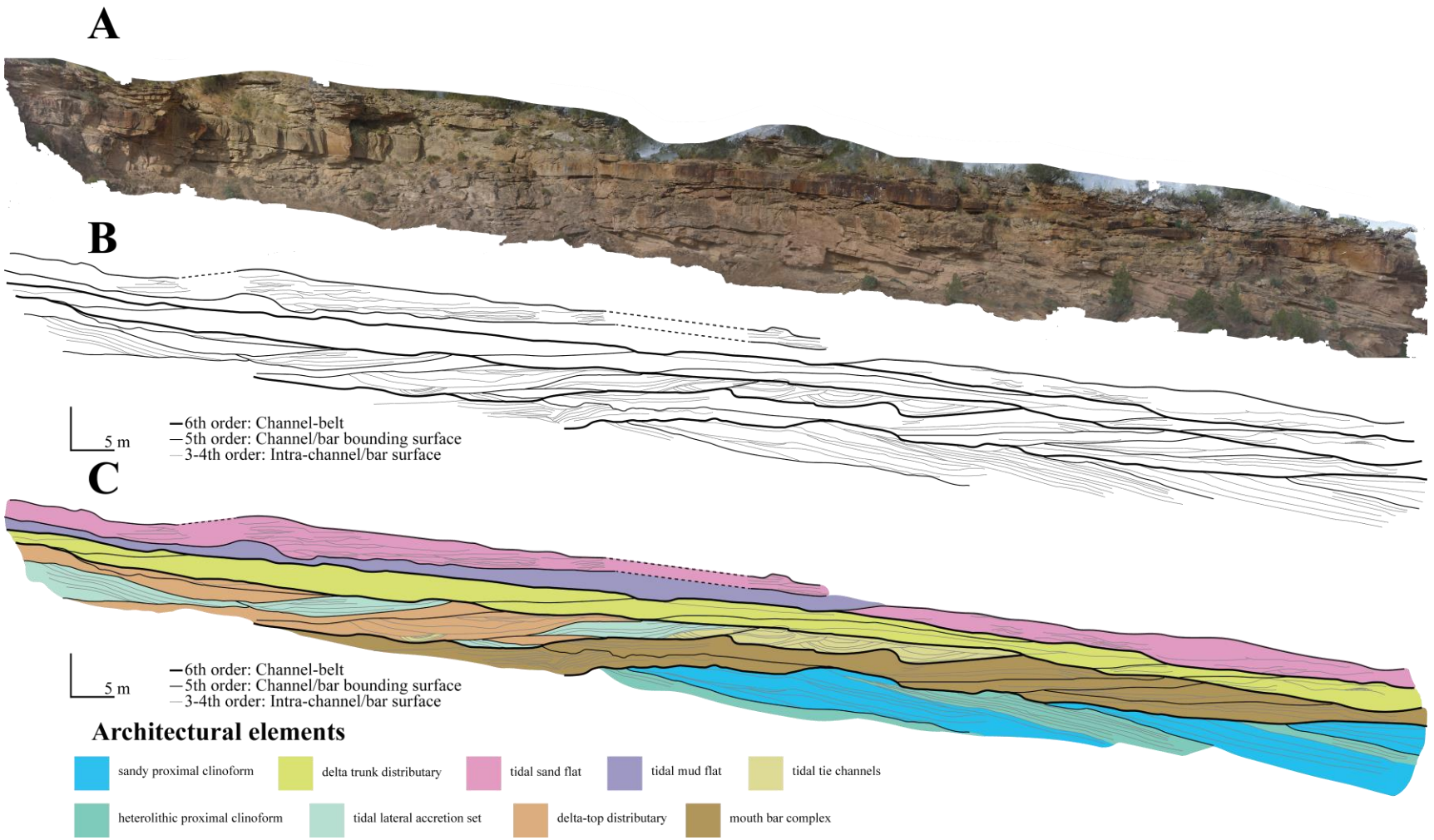
A
B
5 m
6th order: Channel-belt
5th order: Channel/bar bounding surface
3-4th order: Intra-channel/bar surface
C
5 m
6th order: Channel-belt
5th order: Channel/bar bounding surface
3-4th order: Intra-channel/bar surface
Architectural elements
sandy proximal clinoform
delta trunk distributary
tidal sand flat
tidal mud flat
tidal tie channels
heterolithic proximal clinoform
tidal lateral accretion set
delta-top distributary
mouth bar complex

Figure 16: Image of the outcrop studied (A), interpreted bounding surfaces (B), and bounding surfaces with color-coded architectural elements (C) for Thompson Canyon.

Interpretation

Deposits at Thompson Canyon are interpreted as prograding estuarine-bayhead deltaics due to the significant evidence of marine influence. Their progradational nature is apparent with the outcrop becoming more proximal up-section, transitioning from medial delta front to proximal delta front, and is capped by delta plain deposits (Figure 17).

The heterolithic inclined strata are representative of delta clinoforms in the delta front to prodelta transitional zone (A; figure 17). This is interpreted due to its coarsening upwards nature, *Teredolites* burrows, distributary channels, and climbing ripples. These IHS are composed primarily of sand with much smaller layers of interbedded fines and terminal distributary channels locally, placing them in the transition of distal delta front to proximal pro-deltaic environment. *Teredolites* traces lining the basal portion of these sands is indicative of a brackish environment (Nair & Saraswathy, 1971; Giangrande et al., 1994; Distel et al., 2011; MacIntosh et al., 2014; Voight, 2015; Buntin et al., 2022), and preferentially burrow in estuarine environments (Buntin et al., 2022). Observed sands contain climbing ripples, and fines contain evidence of carbonaceous double mud drapes and flaser-lenticular bedding, further placing deposits into a marginal marine environment (Pattison, 2018). The pattern observed of sandy clinoform intervals and muddier clinoform intervals can be attributed to avulsion and migration of distributary channels.

Above the delta front clinoforms lie incisional mouth bar deposits that bevel off the top of the delta clinoforms (B; Figure 17). Mouth bar deposits are observed as massive sandstones with local *Teredolites* burrows at their basal scour with locally observed trough

cross-lamination. Laterally, mouth bar deposits are incised by fluvial channel deposits. These are heterolithic, with muddy layers containing flaser-lenticular bedded mud and sands, local *Teredolites* burrows, bidirectional ripples and cross-stratification, and are interpreted as subaqueous distributary channels on the delta top (C; Figure 17).

Above the mouth bar and subaqueous distributary channel complex lies delta plain deposits. At the base of this interval are laterally stepping and aggrading subaerial distributary channels (D; Figure 17). These channels contain trough cross-bedding transitioning up into rippled surfaces with flaser bedded muds and sands between channel forms. Multiple ripped intervals bound by trough cross-lamination internal to a single channel sheet are indicative of tidal influence and alternating bedforms at high and low tides. Capping this outcrop are tidal sand flat and mud flat deposits (E; Figure 17), containing wavy-bedded sands, flaser-lenticular bedding, carbonaceous laminae, and *Skolithos* in localized sand beds interpreted as tidal sand and mud flats preserved lateral to their equivalent subaerial distributary channel. This up-section transition is consistent with a progradational bayhead delta with deposits becoming more proximal up-section (Figure 17; Aschoff et al., 2018).

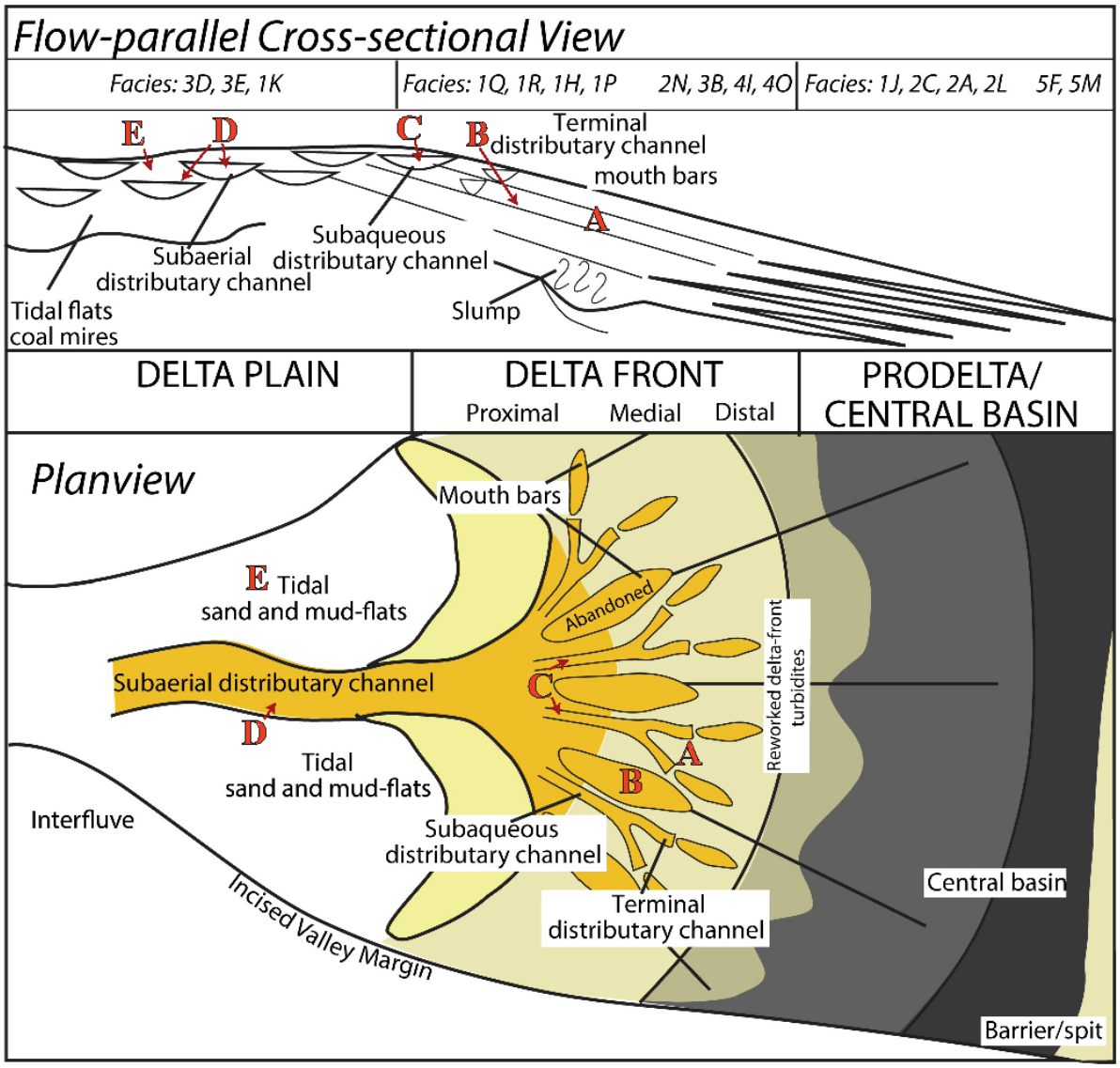

Figure 17: Schematic of bayhead deltas in cross-sectional and planview (Modified from Aschoff et al., 2018). Deposits observed in Thompson Canyon represent medial delta front facies (A) transitioning up-section into proximal delta front facies (B, C) and capped by delta plain (D, E).

Sulfur Canyon:

Sulfur Canyon is the most distal outcrop used in this study, and comprises distal shallow marine deposits in the last reaches of the Castlegate Sandstone. At the base of the outcrop lie interbedded marine muds and very fine sand-siltstone sheets containing

Arenicolites and *Diplocriterion* traces. These deposits show an apparent increase in sand up-section, with thicker sand sheets and reduced spacing between the sands up-section. Localized channel-forms are seen nested within alternating sand and mud sheets. Directly above interbedded marine muds, with no evidence of major incision, lies ~3-5 m of shallow-marine tidally influenced fluvial sandstones along with mud and sand flats. These shallow marine deposits are composed of fine-lower medium sandstone channels containing trough cross-bedding, symmetrical bi-directional ripples, climbing ripples and localized mouth bars. The base of the shallow marine channel system is bound by a 5^{th} order surface representative of a channel belt incision. These channels contain localized lateral *Ophiomorpha nordosa* burrows, iron concretions, *Skolithos*, and bivalve imprints are observed on the upper-most channel-fill tops. Many iron concretions are associated with *Ophiamorpha* burrows, with concretions seen nucleating from an observed burrow.

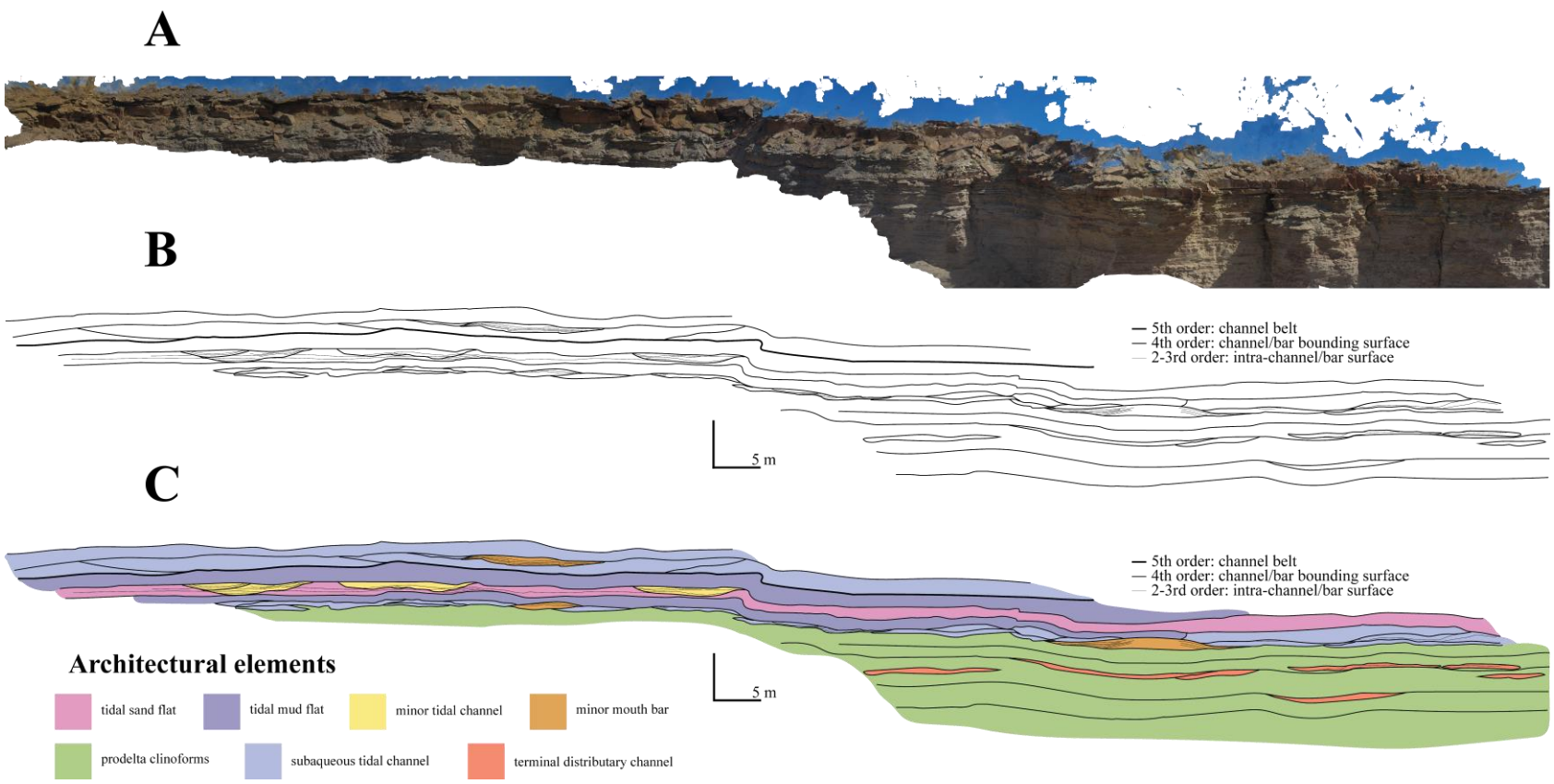
A
B
5th order: channel belt
4th order: channel/bar bounding surface
2-3rd order: intra-channel/bar surface
5 m
C
5th order: channel belt
4th order: channel/bar bounding surface
2-3rd order: intra-channel/bar surface
5 m
Architectural elements
tidal sand flat
tidal mud flat
minor tidal channel
minor mouth bar
prodelta clinoforms
subaqueous tidal channel
terminal distributary channel

Figure 18: Image of the outcrop studied (A), interpreted bounding surfaces (B), and bounding surfaces with color-coded architectural elements (C) for Sulfur Canyon.

Interpretation

The Castlegate Sandstone at Sulfur Canyon represents a prograding shallow marine fluvio-deltaic system with strong imprint of tidal influence. The basal portion of the outcrop is interpreted as a prograding delta front due to their coarsening-up pattern and thinly interbedded layers of tabular shallow marine sands and muds (Aschoff et al., 2018). These thinly interbedded sheets of very fine sands and silty muds contain *Diplocriterion* and *Arenicolites* trace fossils, indicative of a quiet water, nearshore shallow-marine environment (Cornish, 1986; Fürsich, 1974a, 1975; Goldring, 1962, 1964; Mason & Christie, 1986; Oloriz & Rodriguez-Tovar, 2000; Seilacher, 2007; Rodríguez-Tovar & Pérez-Valera, 2013). Locally, terminal distributary channels are seen in this interval that increase in frequency up-section. Overlying these are delta-top facies represented by submarine tidal channels with *Ophiomorpha*, *Skolithos*, and bivalve imprints along with symmetrical ripples and climbing ripples, indicative of a higher-energy environment and shallowing-up from the underlying tabular sand and mud beds. These transition vertically into mud and sand flats, which are indicative of avulsion of the fluvial system sourcing the sands. These delta top strata are tide-dominated, with the shifts from sandier to muddier strata indicative of the fluvial imprint on the tide dominated environment.

These deposits represent the last progradational pulses of the Castlegate Sandstone progradation into the Western Interior Seaway. Compared to outcrops further West, there is much less fluvial influence on the Castlegate strata, and the dominant factor in the observed

outcrop is likely tides. This outcrop is indicative of a sand-poor fluvial system prograding into a shallow, low-accommodation seaway.

3.2) Backwater Length:

In this study, backwater length was calculated using grain-size and average bankfull flow depths based on findings at Woodside Canyon. Flow depths and D_{50} grain sizes were collected from six channels determined to be representative channels for the deposits observed at Woodside Canyon and were collected vertically through the measured section. Flow depth for channels was determined using barforms with full or partial rollover in main trunk-channel deposits within the outcrop. Median grain-size was sampled directly above the thalweg of these representative channel-fill deposits (van Yperen et al., 2021). Using grain size and channel-depth, channel slope was then calculated using equations outlined by Paola & Mohrig (1996) and Holbrook & Wanas (2014). Average slope calculated at Woodside Canyon is 0.000199 m/km (1.99×10^{-4}), consistent with the slope of 0.0002 m/km presented in previous studies (Hampson, 2010; Trower et al., 2018). Backwater length was then calculated using the empirical equation presented by Holbrook & Wanas (2014) and Trampush et al. (2014). The backwater length of 24.1 km presented in this study is consistent with previous studies, which have calculated backwater lengths of ~20 km (Trower et al., 2018) and 20-30 km (Petter, 2010). Data collected present in table 2.

It is likely that backwater length increases as the Castlegate fluvial system progrades East, furthering the downstream evolution and becoming increasingly single-thread. There is an increase in channel depth moving more basinward in the Castlegate system, and likely a reduction of shelf-slope due to infilling of the basin and reduction in accommodation. These factors will likely increase the backwater length of the system, though further data is needed.

Channel	Bankfull depth (m)	D_{50} (mm)	Slope	backwater length (km)
1	5.1	0.35	0.000211	24.2
2	4.8	0.29	0.000185	25.9
3	4.6	0.32	0.000213	21.5
4	5.4	0.34	0.000193	27.9
5	4.1	0.26	0.000195	21.1
Mean	***4.8***	***0.312***	***0.000199***	***24.1***

Table 2: Numbers used for calculations of backwater length from 5 channels at Woodside Canyon. Average bankfull depth (h_b) is 4.8 m. Average D50 is 0.312 mm. Average slope is 1.99×10^{-4} (0.000199), and the resultant average backwater is 24.1 km.

CHAPTER FOUR: Discussion

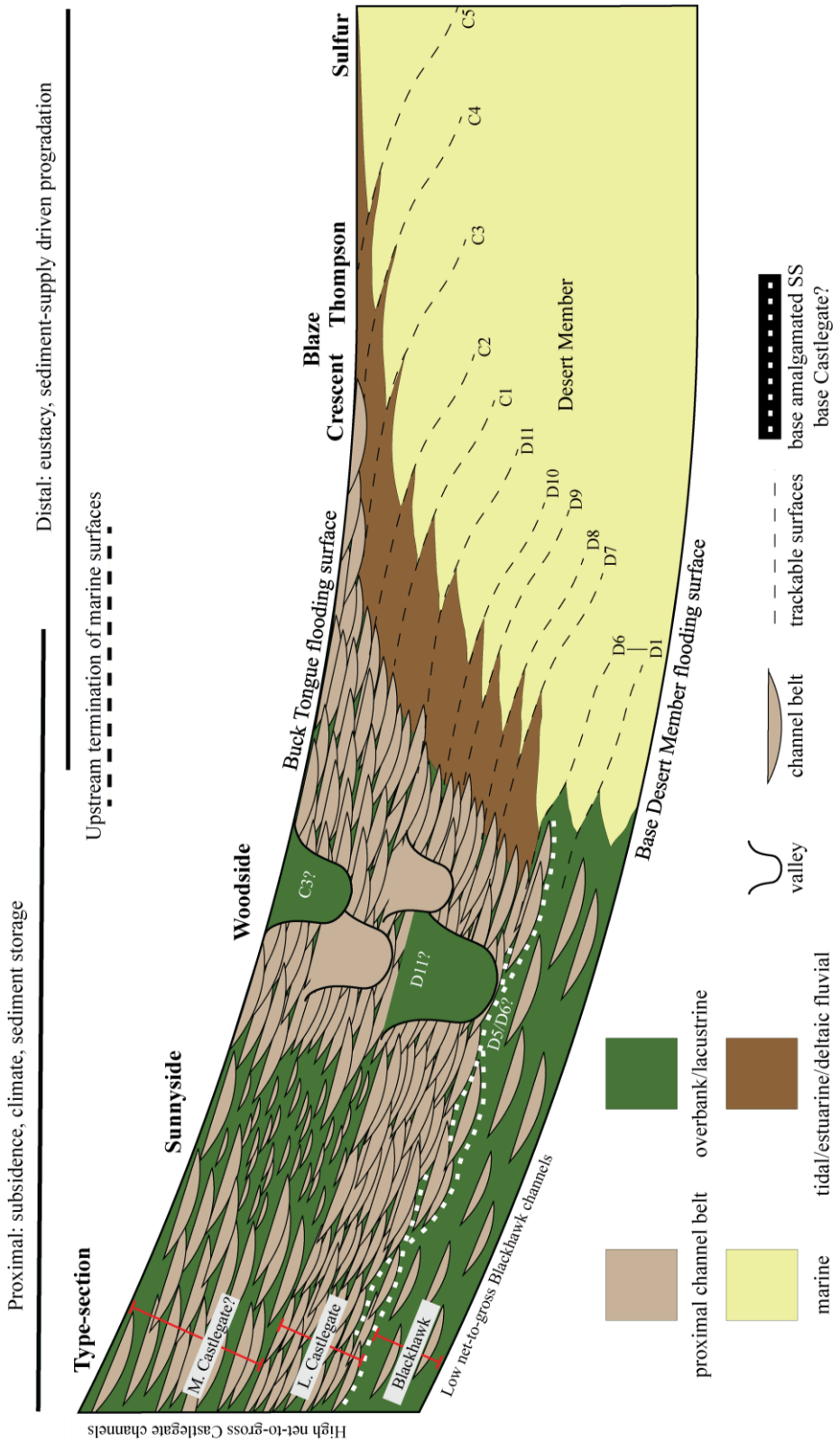

***Figure 19*:** Simplified schematic longitudinal section of the Book Cliffs outcrops of the Castlegate Sandstone into their Desert Member marine equivalent. The base of the amalgamated channel sands typically used to identify the base of the Castlegate Sandstone is often cryptic, and migrates up or down-section by multiple channel stories locally. This indicates that this contact is a regionally conformable, simple facies contact. Sequence stratigraphic surfaces (From Pattison, 2018, 2019a, b, 2020) are trackable from marine strata into the near-shore fluvial, but all regionally trackable surfaces cease to exist up-dip, and are all cryptic, or gone by Woodside Canyon. It is important to note that these outcrops are unlikely representative of one continuous fluvial system.

4.1) Trackable Surfaces

The base of the Castlegate Sandstone is not representative of a surface that is trackable throughout the Castlegate fluvial system (Figure 19), it is simply an observed lithostratigraphic contact comprising discontinuous, local scour contacts. From the proximal to medial reaches of the Castlegate the base of the sandy, amalgamated fluvial deposits interfinger with the underlying, flood-plain rich Blackhawk strata (Pattison, 2020). This is best exemplified in the proximal reaches of the Castlegate such as the type-section (Pattison, 2020) to Woodside Canyon, where laterally, floodplain rich fluvial deposits are observed interfingering laterally with the amalgamated channel sheet that is typically identified as the Castlegate Sandstone (Figure 13). These observations agree with previous interpretations that place the base of the Castlegate amalgamated fluvial sands as a simple facies contact within a progradational system due to an increase in sand supplied to the basin (Hajek and Heller, 2012; Howell et al. 2018; Pattison, 2018, 2019 a, b, 2020; Pettit et al., 2019; Chamberlin and Hajek, 2019, 2022) and that the same fluvial system created both the Castlegate and uppermost Blackhawk fluvial strata (Adams & Bhattacharya, 2005; Pettit et al., 2019).

It is unlikely that the exposure of Castlegate outcrops are consistent with one single down-stream fluvial system (Figure 20; Miall, 2001; Petter, 2010; Pattison, 2018; Pettit et al.,

2019; Sundell et al., 2024), further making possible sequence stratigraphic surfaces either cryptic, or confined to regions of the outcrop belt. Zircon data along the Wasatch Plateau shows three distinct tributary systems in the Castlegate Sandstone, with the type-section, Joe's Valley Reservoir, and Salina Canyon each representing a different transect of the larger Castlegate fluvial system (Pettit et al., 2019; Sundell et al., 2024). Paleocurrent directions within these proximal tributaries also show varying orientations (Miall, 2001; Pattison, 2018), and do not connect into one continuous downstream profile.

It is possible that stratigraphic surfaces are solely expressed in an individual transect, as each transect is likely responding to different allogenic drivers. This is apparent in the proximal outcrops in this study, which have differing architectures, varying levels of incision and aggradation, and different facies distributions (Figure 20). The Castlegate type-Section shows much higher rates of aggradation, with most barforms showing full or near-full preservation throughout (Hajek & Heller, 2012; Chamberlin & Hajek, 2019, 2022; Mitten et al., 2020). Joe's Valley show much lower levels of barform preservation (Chamberlin & Hajek, 2019), valley-scale incisions, and thick overbank successions preserved on valley terraces. Lastly, Salina Canyon shows a greatly different architecture, composed of fluvial sheets with much higher rates of incision, and very little overbank preservation. This is similar to observations made in the up-dip reaches of the Ganges-Brahmaputra system, where tributaries responding to varying tectonic controls, resulting in differing architecture and levels of incision, overbank preservation, and fluvial style (Goodbred & Kuehl, 1998; Goodbred & Kuehl, 2000; Goodbred et al., 2003).

The Castlegate Sandstone shows no evidence of backwater influence from Woodside Canyon and further up depositional dip (Figure 20). This is based on the backwater length of

~24 km (Table 2), and the correlation of the D6 parasequence to the lowermost Castlegate amalgamated sands at Woodside Canyon (Pattison, 2020). Woodside Canyon remains >24 km away from the furthest up-dip appearance of coeval shoreface strata (Figure 21), and therefore remains outside of the backwater reach. All exposure of the Castlegate Sandstone West of Woodside Canyon is not influenced by backwater effects.

Architecture and fluvial style of the Castlegate Sandstone varies greatly from the proximal reaches, to the distal reaches within backwater length. Outcrops from Woodside Canyon West consist of stacked braided fluvial channel-belt deposits with prevalent downstream accreting barforms (Miall, 1995; Olsen et al., 1995; Mclaurin & Steel, 2007; Hajek & Heller, 2012; Chamberlin & Hajek, 2019, 2021; Mitten et al., 2020). Despite their primarily braided nature, there is still a recorded downstream increase in sinuosity (Mitten et al., 2020) and increase in flow-depth attributed to the downstream evolution of the system (Holbrook et al., 2006; Li et al., 2015; Mitten et al., 2020). Changes in architecture down depositional dip are also attributed to a reduction in subsidence rates, resulting in an increase in incisional surfaces (Mitten et al., 2020). Within these proximal outcrops, there is not any on through-going surface that can be tracked regionally, or even through continuous, long outcrops (Hajek & Heller, 2012; Pattison, 2020), and the base Castlegate is cryptic (Figure 19; Pattison, 2020).

Distal outcrops of the Castlegate Sandstone comprise moderate to high sinuousity meandering channels nested in backshore muds, or shoreface-incising tidal-estuarine channel-forms. These deposits are typically low-accommodation, showing primarily lateral amalgamation rather than the vertical stacking observed in the proximal reaches. This is similar to the low-accommodation, laterally amalgamating channels observed in the Mesa

Rica Sandstone of the Dakota Group (Holbrook, 2006; van Yperen, 2021), which are within backwater reach, and driven by autogenic flood-induced scour by backwater hydrodynamics (Holbrook, 2006; van Yperen, 2021).

All incisions observed within the Castlegate Sandstone in its distal reaches are consistent with that of autogenic scouring, with the largest scours induced by backwater hydrodynamics during flood (Trower et al., 2018). A similar argument was made for the Mesa Rica Sandstone, where valleys within backwater length are incised via autogenic flooding processes (Holbrook, 1996, 2006; van Yperen et al, 2021). The autogenic nature of these valley-scale scours removes the need to induce sea-level drop to explain valley formation. This results in no IVF systems to be tracked up-dip with the exception of parasequence C3, the only parasequence where progradation is likely tied to sea-level drop (Figure 20; Pattison, 2020). These autogenic scour surfaces driven by backwater hydrodynamics would not be expressed outside of the backwater length, and therefore will cease to exist near the up-dip reaches of backwater influence (Bull, 1991; Blum, 1993; Guccione, 1994; Shanley & McCabe, 1994; Tornqvist, 1998; Blum & Tornqvist, 2000; Holbrook et al., 2001, 2006; van Yperen 2021, 2024).

Many studies have attempted to track sequence stratigraphic surfaces from the distal Castlegate strata up-dip into the proximal reaches (Van Wagoner, 1991, 1995; Miall, 1993, 2014, 2016; Yoshida et al., 1996, 1998; Willis, 2000; Yoshida, 2000; Miall & Arush, 2001a, b; Hettinger & Kirschbaum, 2002; Seymour & Fielding, 2013; Hampson, 2016). This is most likely not possible, as the proximal reaches of the Castlegate do not respond to the same sea-level drivers as the distal reaches of the system. Sediment supply is argued as a large driving factor on large-scale architecture within the proximal and distal Castlegate (Pattison, 2018;

Chamberlin & Hajek, 2019), but the responses to this increase in sediment supply vary greatly across depositional dip. In proximal reaches, such as the type-section, sediment capture is the main result of increased sediment supply due to the high rates of subsidence (Mitten et al., 2020). High levels of sediment capture at the type-section are supported by evidence showing few incisional surfaces, and high levels of bar preservation within the highly aggradational unit (Hajek & Heller, 2012; Chamberlin & Hajek, 2019, 2021; Mitten et al, 2020), which is resultant of the high subsidence rates recorded at this location (Mitten et al., 2020). Down-dip, this same increase in sediment supply is expressed through progradation of marine shoreface equivalents with minimal aggradation (Pattison, 2020). Fluvial sequence stratigraphic surfaces down-dip migrate a limited distance up-dip with the upstream propogation controlled by backwater length, slope, and the magnitude of the eustatic rise or fall (Bull, 1991; Blum, 1993; Guccione, 1994; Shanley & McCabe, 1994; Tornqvist, 1998; Blum & Tornqvist, 2000). There is no reason that a single, through-going sequence boundary should be created from a low-accommodation prograding nearshore fluvial channels and shoreface package within backwater length to a high-accommodation, aggradational stack of fluvial channels up-dip (Bull, 1991; Blum, 1993; Guccione, 1994; Shanley & McCabe, 1994; Tornqvist, 1998; Blum & Tornqvist, 2000).

Architectures from Woodside Canyon and further West are reacting solely to subsidence rates, sediment supply, and autogenic factors such as avulsion rates, patterns and fluvial style. No influence of sea-level should be expected to be observed this far up-dip (Figure 20). Distal Castlegate strata are also reacting to avulsion rates and patterns, but these patterns are extremely different due to the down-stream evolution of the Castlegate fluvial system (Holbrook et al., 2006; Li et al., 2015; Mitten et al., 2020) with the strongest drivers

of fluvial architecture down-dip being sea-level and sediment supply (Pattison, 2018; Trower et al., 2018). Many of these shoreface-incising channels are likely representative of a distributive fluvial system prograding over a shallow shelf (Pattison, 2018).

It is to be expected that within the longitudinal profile of a fluvial system sequence stratigraphic surfaces should eventually cease to correlate, as different portions of the basin are subject to very different conditions and architectural drivers (Strong & Paola, 2008; Martin et al., 2009; Holbrook & Bhattacharya, 2012). Fluvial surfaces, such as the base of the Castlegate Sandstone, are diachronous surfaces that are created over time (Holbrook & Bhattacharya, 2012). These surfaces may not be unconformities, nor do they represent a time-surface, and may only be present locally, and may not be correlative (Holbrook, 2010; Bhattacharya, 2011; Holbrook & Bhattacharya, 2012). It is well recorded that fluvial deposits may be preserved during low-stand rather than producing a bypass surface (Tornqvist et al., 2000; Makinouchi et al., 2001; Wallinga et al., 2004; Blum & Aslan, 2006; Sylvia & Galloway, 2006), and that that valley scale surfaces may be present up-dip, or down-dip, but do not have to be correlative between the two (Bhattacharya, 1993; Holbrook, 2001; Posamentier, 2001; Wellner & Bartek, 2003; Holbrook et al., 2006; Gibling et al., 2011).

This disconnect between up and down-dip surfaces is well documented in the Ganges-Brahmaputra river sediment and delta (Goodbred & Kuehl, 1998; Goodbred & Kuehl, 2000; Goodbred et al., 2003) where up-dip coarse-grained fluvial facies are dominantly controlled by tectonics and subsidence, whereas distal deltaic facies are primarily dominated by eustatic fluctuation and sediment supply. Sequence stratigraphic surfaces in the modern Ganges-Brahmaputra delta cannot be correlated up-dip as age-dating of sediment flux makes apparent (Goodbred & Kuehl, 1998). It should be expected that such surfaces will

not be trackable and continuous in the longitudinal profile of fluvial systems within the ancient rock record.

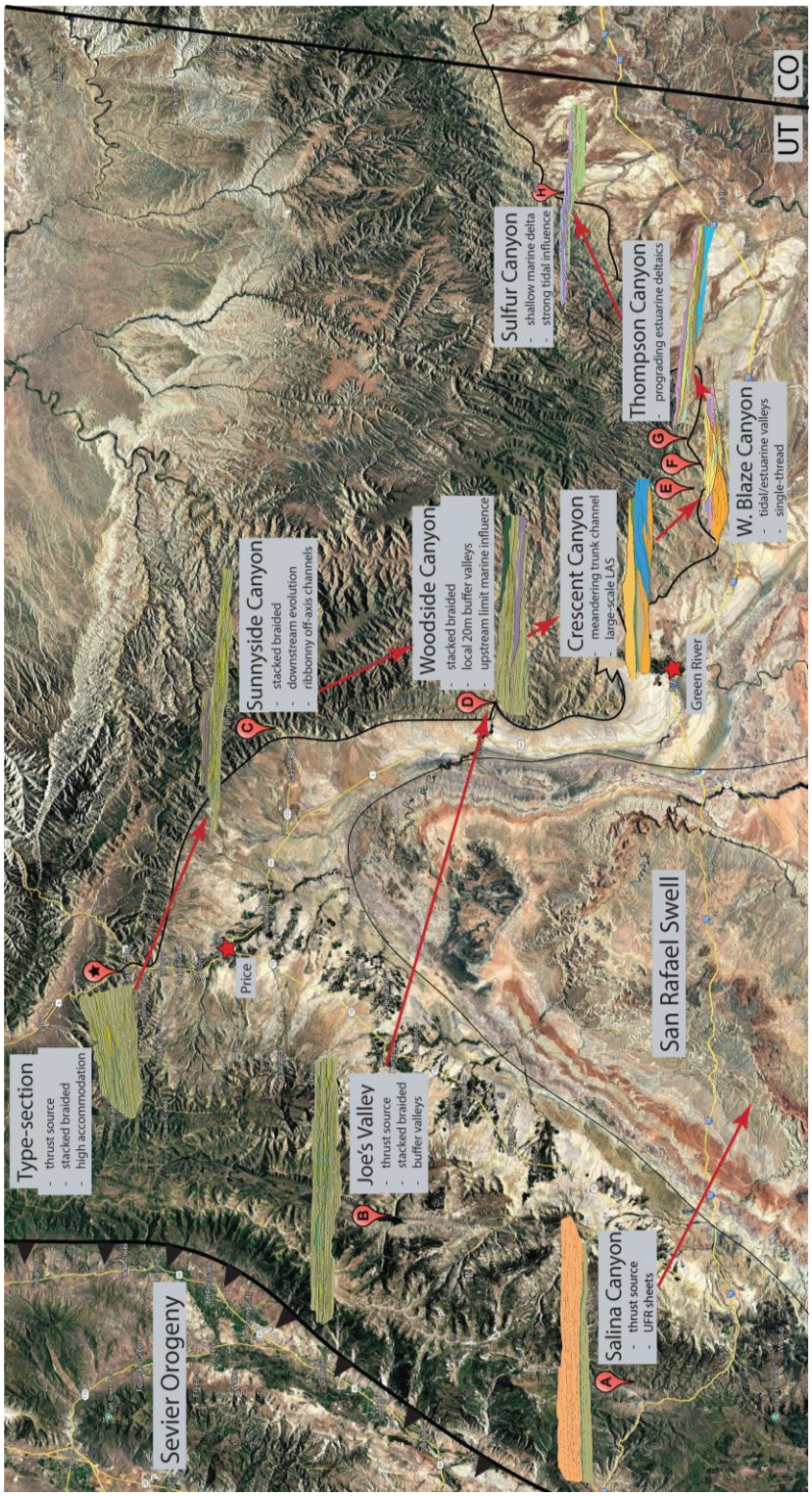

***Figure 20*:** Outcrop orthomosaics overlain on google earth imagery of the Book Cliffs, UT. Main features and unique architectures listed for each outcrop. Red arrows represent downstream connectivity of tributary systems. Each proximal outcrop (Salina, Joe's Valley, type-section) represents a different tributary system with Salina Canyon not feeding Castlegate outcrops further the East (Pettit et al., 2019).

4.2) Valleys at Woodside Canyon

Woodside Canyon expresses valley fills representing repeated individual periods of incision and subsequent valley-scale filling. These valleys are isolated, and stacked vertically up-section and each represent individual periods of scour and subsequent aggradation in successive order. Valleys at Woodside Canyon are local, and were not observed anywhere else longitudinally within the Castlegate strata. Possible drivers for valley scale incision of this caliber include tectonic uplift, up-dip migration of a buffer knick-point due to eustatic sea-level drop, or discharge-related river-incisional cycles. The true driver of these incisions is still unclear, though some possibilities can be negated.

Valleys observed at Woodside Canyon are likely not the result of tectonics. If tectonic uplift were the driver of valley incision at Woodside Canyon, incision would be expected to be observed originating from one significant surface and would be present for an extended range along depositional dip if from more than more than local faulting. A surface that is trackable up-dip is not observed, nor are local faulting or other coeval records of deformation to support this model. With multiple recorded incision and fill events stacked vertically up-section, this would necessitate inducing repeated individual uplift events with subsequent relaxation on scales of several meters to create each individual valley scour. These scours occur on a timeframe shorter and larger than expected of tectonic events, are not clustered on

a singular surface, and are not observed up-dip, so they are likely not induced by basin tectonics.

Valleys at Woodside Canyon are not indicative of backwater induced scours. There is no backwater influence observed within the Castlegate amalgamated sands in Woodside Canyon, therefore the base-Castlegate in these deposits may coincides at the earliest with parasequence D6 (Figure 16, Pattison, 2020), the first parasequence where this location would be greater than one backwater length from the paleo-shoreline. Incised valleys are observed up-section in this interval, so they are expected to be incised much later than parasequence D6. These valleys cannot be induced by backwater scour hydrodynamics due to their distance of significantly greater than the calculated ~24 km backwater length from the first appearance of the shoreline and the lack of observed backwater influence.

The Castlegate Sandstone at Woodside Canyon is likely within the range of knick-point migration for part of the vertical section, though knick-point migration is not the source of incision. As observed in the Mesa Rica Sandstone of the Dakota Group, the up-dip knick-point caused by eustatic sea-level drop scales to ~2x backwater length in the system (van Yperen et al., 2020). This is confirmed by modern studies of the Mississippi where Holocene sea level drop caused kick-point migration to ~1.7 backwater lengths (Rittenour et al., 2007; Blum, 2013) with knick-point valleys typical of fluvial systems (van Yeprin et al., 2024). Applying this to the Castlegate, the maximum migration of a knick-point and valley-scale incision would most likely be ~48 km though possibly up to ~60 km up-dip from the paleo-shoreline of any given parasequence based on a ~24.1 km backwater length as calculated in this study, and the 20-30 km backwater length calculated in other studies (Trower et al., 2018; Petter, 2010).Based on a knick-point migration of 2x backwater length, the Castlegate

Sandstone in Woodside Canyon was very likely within reach of up-dip knick-point migration from parasequences D6-D10 using the more conservative 20 km estimate of backwater length. If backwater length is increased to 30 km, up-dip kickpoint migration would be ~60 km, and able to reach Woodside Canyon from parasequences D6-C3 (Figure 20). The Woodside Canyon section is at or near the up-dip limit of sea-level influence in all cases.

Valleys observed at Woodside Canyon cannot be induced by eustatic sea-level drop and knick-point migration. Despite Woodside Canyon being at times within two backwater lengths of the paleoshoreline, there is no evidence in distal strata of the type of large-scale sea-level drops that would account for the observed scale and frequency of valley incision. Given a maximum recorded scour depth is 20 m and average recorded channel depth at this location is 4.8 m, the water surface would be 15.2 m below the surrounding topography (scour depth – channel depth). A eustatic origin for this incision requires inducing at least a 15.2 m drop in sea-level, and with a shelf slope of 0.0002 m/km would require the shoreline to migrate ~76 km to the East. Sea level drop of this scale is not observed in the distal Castlegate strata, nor is a 70+ km shoreline progradation or incised valley cutting through distal strata, therefore, the valleys in Woodside Canyon could not have been induced by sea-level drop and knickpoint migration.

Parasequences are associated with bounding flooding surfaces that record landward flooding (Van Wagoner, 1990) but are not generally associated with large sea level rises or falls in the Castlegate and equivalent Desert Member (Pattison, 2020). The exception is parasequence C3-C4 (Pattison, 2020), which does record a measurable shoreface downstep associated with sea level drop. The C3-C4 parasequence progrades 11.6 km with a shoreline trajectory of 0.025º (-0.44 m/km) (Pattison, 2020), resulting in an induced sea-level drop of

5.06 m, and should dissipate up-dip (Blum, 1993; Holbrook & Bhattacharya, 2012). This 5.06 m sea-level drop much smaller than the 15.6 m sea-level drop necessary to incise the valley observed at Woodside Canyon. The multiple valleys observed would each require their own sea-level drop, which is not recorded in equivalent downdip shoreline strata by any study.

It is unlikely that valley scours at Woodside Canyon coincide with the confluence of the southern and northern transects of the Castlegate fluvial system. First, they comprise multi-story fill and not the single-story fill expected from an overdeepened single channel formed at a confluence scour. Given the observed scour depths of 12-20 m and 4.8 m average bankfull depth, these scours are well within the 4-5x increase in scour depth observed at the river confluence in the modern braided Jumana River in Bangladesh (Best & Ashworth, 1997). The localized nature of these scours favors flood at river confluence as the driver of these large incisions, as they are not observed at any nearby Castlegate outcrops. Scours for the Jumana River having an observed increase in scour depth for only a 2 km distance downstream from the confluence (Best & Ashworth, 1997), so these scours would be expected to be confined to Woodside Canyon, though the multi-story valley-fill, the repetitiveness of valleys vertically, and the high depth of the valleys makes this explanation improbable.

The Woodside Canyon section is likely shortly down-dip of the confluence of the northern and Southern transects of the Castlegate fluvial system. Provenance evidence (Pettit et al, 2019) and increase in grain-size from Sunnyside to Tusher Canyon (Petter, 2010) confirms that the northern and southern transects of the Castlegate have joined by Tusher Canyon, just 15 km East of Woodside Canyon. The location of the confluence of these

systems has not been defined specifically. This means, however, that the confluence of the two transects must have occurred between Sunnyside and Green River, in which Woodside Canyon is situated. An in-depth provenance study up-section at Woodside Canyon must be undertaken to definitively determine whether the northern and southern transect confluence is up-dip of Woodside Canyon. If no evidence of mixing of parent rivers is found, it is possible that valleys at Woodside Canyon are representative solely of the southern transect of the Castlegate fluvial system. The southern transect which lacks outcrop exposure from Joe's Valley to Woodside Canyon owing to uplift and erosion from rise of the San Rafael Swell. In this case, it is possible that valleys observed in Woodside Canyon may have been expressed up-dip in the southern transect, though these deposits have since been removed.

Given the lack of evidence for tectonic or eustatic drivers, valleys observed in Woodside Canyon are likely evidence of monsoon-driven flood scour. These flood scours are resultant of an increase in discharge from the confluence of the Northern and Southern transects of the Castlegate system, resulting in larger scours during flooding periods. Up-dip from Woodside Canyon, the subsidence rates are significantly higher (Mitten et al., 2020), making incision less likely. Discharge in individual tributaries to the overall system is likely not high enough to cut valley incisions given the high subsidence rates recorded up-dip, where down-dip of the confluence, increase in discharge during flooding is amplified. Buffer valleys are typically controlled by sediment or water discharge within the system (Holbrook et al., 2006, Bhattacharya, 2011), and are resultant of the fall of the equilibrium profile of the channel because of upstream controls (Mackin, 1948; Lane, 1955; Paola, 2000; Blum & Tornqvist, 2000; Milana & Tietze, 2002; Van Den Berg et al., 2008). At Woodside Canyon, it is probable that substantial increase in water discharge during flooding periods within the

well-documented monsoonal climate caused the valleys documented in this study. These buffer valleys are expected to taper down-dip (Holbrook, 1996, 2001; Posamentier, 2001; Weissman et al., 2002; Wellner and Bartek, 2003; Bhattacharya, 2011), which is documented in the Cretaceous Dakota Group where valleys of four-times deeper than channel-fill elements taper into single-story incisions near the shoreline (Holbrook, 1996, 2001). Similar valley incisions resultant of up-stream increase in discharge are observed in experimentally controlled valleys (Milana & Tietze, 2002; Van Den Berg et al., 2008), the Ferron Sandstone (Garrison & Van Den Bergh, 2006; Li et al., 2010), and Quaternary valleys of the San Joaquin River (Weissman et al., 2002; Weissman et al., 2005). This would explain the lack of valleys of scale comparable to this in the down-dip reaches of the system, leaving these valleys confined to the buffer-zone up-dip and tapering out towards the shoreline (Holbrook, 2001, 2006; Holbrook & Bhattacharya, 2014).

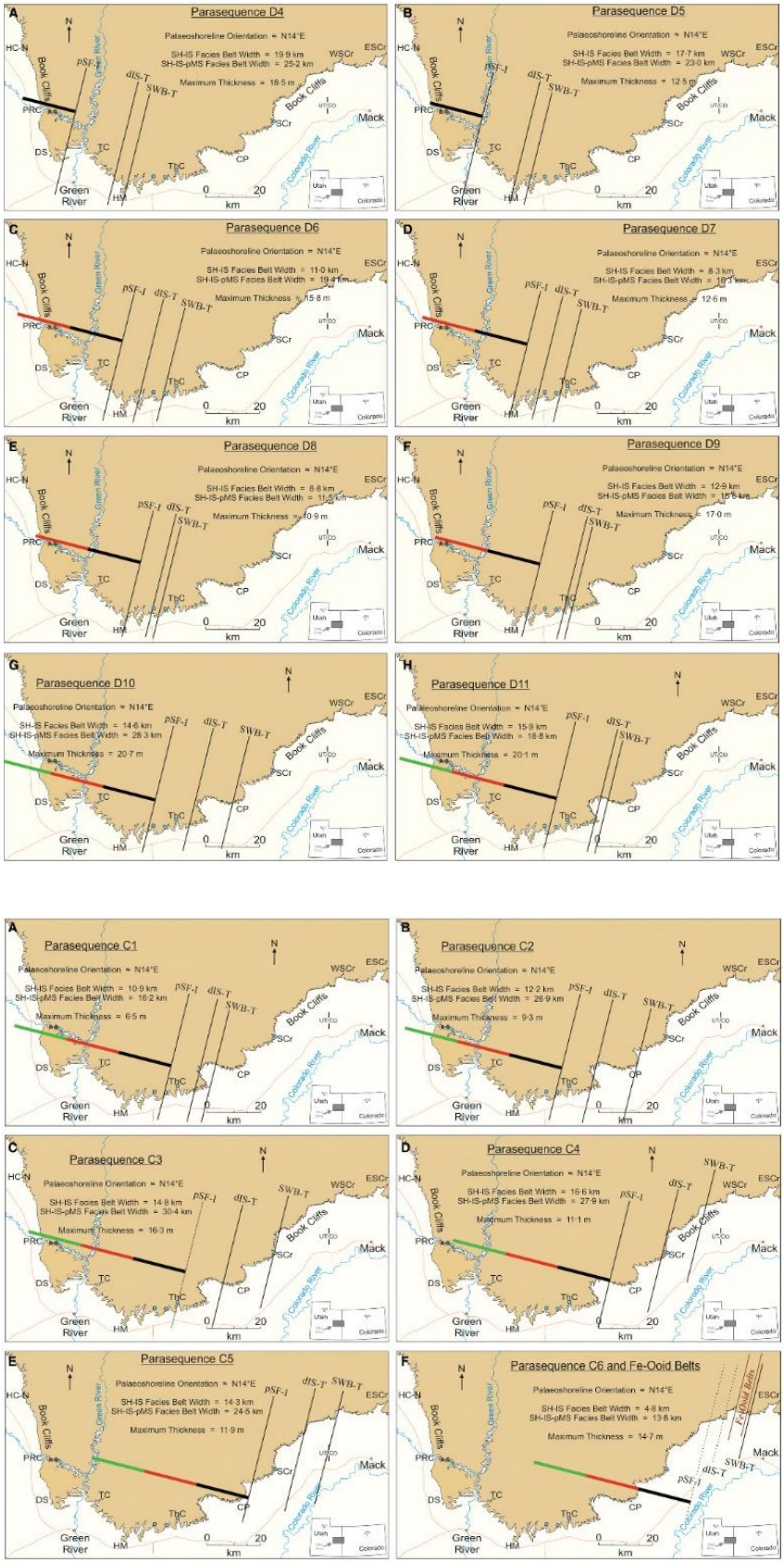
A
Parasequence D4
Palaeoshoreline Orientation = N14°E
SH-IS Facies Belt Width = 19·9 km
SH-IS-pMS Facies Belt Width = 25·2 km
Maximum Thickness = 18·5 m
B
Parasequence D5
Palaeoshoreline Orientation = N14°E
SH-IS Facies Belt Width = 17·7 km
SH-IS-pMS Facies Belt Width = 23·0 km
Maximum Thickness = 12·5 m
C
Parasequence D6
Palaeoshoreline Orientation = N14°E
SH-IS Facies Belt Width = 11·0 km
SH-IS-pMS Facies Belt Width = 19·4 km
Maximum Thickness = 15·8 m
D
Parasequence D7
Palaeoshoreline Orientation = N14°E
SH-IS Facies Belt Width = 8·3 km
SH-IS-pMS Facies Belt Width = 18·1 km
Maximum Thickness = 12·6 m
E
Parasequence D8
Palaeoshoreline Orientation = N14°E
SH-IS Facies Belt Width = 8·8 km
SH-IS-pMS Facies Belt Width = 11·5 km
Maximum Thickness = 10·9 m
F
Parasequence D9
Palaeoshoreline Orientation = N14°E
SH-IS Facies Belt Width = 12·9 km
SH-IS-pMS Facies Belt Width = 15·6 km
Maximum Thickness = 17·0 m
G
Parasequence D10
Palaeoshoreline Orientation = N14°E
SH-IS Facies Belt Width = 14·6 km
SH-IS-pMS Facies Belt Width = 28·3 km
Maximum Thickness = 20·7 m
H
Parasequence D11
Palaeoshoreline Orientation = N14°E
SH-IS Facies Belt Width = 15·9 km
SH-IS-pMS Facies Belt Width = 18·8 km
Maximum Thickness = 20·1 m
A
Parasequence C1
Palaeoshoreline Orientation = N14°E
SH-IS Facies Belt Width = 10·9 km
SH-IS-pMS Facies Belt Width = 16·2 km
Maximum Thickness = 6·5 m
B
Parasequence C2
Palaeoshoreline Orientation = N14°E
SH-IS Facies Belt Width = 12·2 km
SH-IS-pMS Facies Belt Width = 26·9 km
Maximum Thickness = 9·3 m
C
Parasequence C3
Palaeoshoreline Orientation = N14°E
SH-IS Facies Belt Width = 14·8 km
SH-IS-pMS Facies Belt Width = 30·4 km
Maximum Thickness = 16·3 m
D
Parasequence C4
Palaeoshoreline Orientation = N14°E
SH-IS Facies Belt Width = 16·6 km
SH-IS-pMS Facies Belt Width = 27·9 km
Maximum Thickness = 11·1 m
E
Parasequence C5
Palaeoshoreline Orientation = N14°E
SH-IS Facies Belt Width = 14·3 km
SH-IS-pMS Facies Belt Width = 24·5 km
Maximum Thickness = 11·9 m
F
Parasequence C6 and Fe-Ooid Belts
Palaeoshoreline Orientation = N14°E
SH-IS Facies Belt Width = 4·8 km
SH-IS-pMS Facies Belt Width = 13·8 km
Maximum Thickness = 14·7 m
Fe-Ooid Belts
N
HC-N
Book Cliffs
Green River
PRC
DS
TC
TbC
HM
CP
WSCr
ESCr
SCr
Mack
Colorado River
PSF-I
dIS-T
SWB-T
0
20
km
Utah
Colorado

***Figure 21*:** Shoreline trajectories for Desert Member and Castlegate parasequences (Modified from Pattison, 2020). Black, red, and green lines all represent 20 km, and backwater length is calculated at ~24 km. Black line is within 20 km of first appearance of thick-bedded shoreface sandstone (Pattison, 2020), and lies within backwater reach. Red line is 20-40 km, and is within 2x backwater reach. Green indicates 40-60 km from the first appearance of the shoreface deposits, and if backwater is >20 km, it may be within two backwater lengths. Red star represents Woodside orthomosaic location, green star is Woodside measured section. Blue circles represent outcrop locations at Crescent, W. Blaze, Thompson, and Sulfur Canyons, listed from West to East.

4.3) Climate

The Castlegate Sandstone in the proximal to medial reaches shows evidence of an up-section change in climate resulting in increased stream power and of large flooding events. The Campanian WIS was dominated by monsoonal climate with highly variable temperatures and precipitation (Kump & Slingerland, 1999; Poulsen et al., 1999; Poulsen et al., 2007; Fricke et al., 2010; Foreman et al., 2011; Sewall & Fricke, 2013; Dennis et al., 2013; Burgener et al., 2019; Curley et al., 2025). Evidence for this as a primary driver of architectural variation within the Campanian Castlegate Sandstone are previously overlooked.

Evidence for a climatic shift is observed up-section in nearly all proximal-medial Castlegate outcrops with the exception of Sunnyside Canyon, though this is likely a reflection of poor exposure. The upper portion of the Castlegate at Sunnyside Canyon is primarily covered, and interpreted as small distributary channels away from the main channel belt. The patterns here likely reflect temporal diversion of flow into a non-trunk area, rather than major changes in discharge because of large-scale climatic shifts.

All outcrops in the proximal reaches of the Castlegate express an up-section increase in discharge and flooding events. Evidence is seen in Salina Canyon with the observed

transition from lower-flow regime strata at the base of the outcrop transitioning up-section into upper-flow regime dominated sheets. Dominance of upper flow regime channels is widely cited as evidence for flashy discharge, and a fluvial system driven by large flooding events (Fielding, 2006; Plink-Bjorklund, 2015; Walker & Holbrook, 2022) which increases in frequency up-section at Salina Canyon (Figure 7, Figure 8). Bankfull flood size and bed shear stress also increase up-section. Evidence at Joe's Valley includes an up-section increase in channel depth, and climate induced buffer valley scours, along with localized occurrence of channel fills with substantially increased local grain-size. The Castlegate type-section shows similar increase in channel depth (Hajek & Heller, 2012; Chamberlin & Hajek, 2019; Mitten et al., 2020). An observed increase in frequency and scale convoluted bedding is also recorded Salina Canyon, Joe's Valley Reservoir, and the Castlegate type-section.

Deposits at Woodside Canyon contain evidence of large-scale scours of up-to 20 m deep driven by climatic shifts altering discharge. These valleys are observed incising only from the upper-section of the outcrop in Woodside Canyon. Up-section increase in coaly material in measured sections and coaly lacustrine deposits infilling the largest observed Woodside valley-scale scour are potentially indicative of an increasingly wet environment. Distal outcrops of the Castlegate Sandstone down-dip of Woodside Canyon commonly record scours greater than a single channel story resultant of flood-induced scour within backwater length (Trower et al., 2018). These operate on a timescale of less than a parasequence, thus is much too short to be induced by large-scale tectonics. Valley scours in the proximal areas are similar in timing, but are too far up dip to be sea-level driven, and appear rapid and large for tectonic drivers. This argues that these valleys are climatically driven by upstream changes in discharge vs sediment supply (Holbrook et al., 2006).

CHAPTER FIVE: Conclusions

- The Castlegate Sandtone records an increasingly flashy discharge and larger discharge up-section in proximal/up-dip reaches, arguing for intensification of the Campanian Monsoon over the duration of Castlegate deposition.
- Outcrops at Salina Canyon, Joe's Valley Reservoir, and the Castlegate type-section are independent tributary systems with varying architectures and levels of incision and aggradation between them based on slope, discharge, and subsidence rates.
- Salina Canyon drainage is representative of coarse-grained upper-flow regime sheet channel deposits likely reflecting highly flashy discharge, in contrast to the Castlegate type-section and Joe's Valley drainages, which are consistent with more typical stacked-braided channel systems.
- The Castlegate Sandstone from proximal outcrops down-dip to Woodside Canyon is responding to up-dip controls including sediment supply, discharge, and subsidence rates, whereas distal/down-dip outcrops record response to sediment supply, and eustatic sea-level. Subsidence rates reduce down-dip, and the effect of sea-level is gone up-dip by Woodside Canyon, resulting in lack of correlative sequence-stratigraphic surfaces linking proximal and distal locations.
- Valleys at Woodside Canyon are at the margins of up-dip eustatic control, do not correspond with sea-level falls, and were not induced by sea-level drop.
- Large cut-and-fill episodes observed in Woodside Canyon are likely due to climate driven flood-induced scour and fill cycles of the Castlegate fluvial system i.e., up-dip controlled buffer valleys. Large-scale cut-and-fill events as observed here are not seen elsewhere in the Castlegate.

- Deposits in Thompson Canyon are consistent with the true incised valley fill model related to sea-level drop, with a valley cut into marine strata during a sea-level low being infilled with prograding estuarine deltaic deposits deposited during a subsequent sea-level rise. This contrasts with the climate driven incisional valleys farther up dip at Woodside Canyon.
- The Castlegate Sandstone transitions from high-accommodation braided channels in its proximal reaches to isolated, low-accommodation moderate-high sinuousity meandering and shoreface incising distributary channels in the distal reaches, with channel depth increasing substantially down-dip.

References

Alexander, J., & Fielding, C. (1997). Gravel antidunes in the tropical Burdekin river, Queensland, Australia. *Sedimentology*, *44*(2), 327-337.

Armstrong, R. L. (1968). Sevier orogenic belt in Nevada and Utah. *Geological Society of America Bulletin*, *79*(4), 429-458.

Aschoff, J., & Steel, R. (2011). Anomalous clastic wedge development during the Sevier-Laramide transition, North American Cordilleran foreland basinUSA. *Bulletin*, *123*(9-10), 1822-1835.

Aschoff, J. L., Olariu, C., & Steel, R. J. (2018). Recognition and significance of bayhead delta deposits in the rock record: A comparison of modern and ancient systems. *Sedimentology*, *65*(1), 62-95.

Alexander, J., Bridge, J. S., Cheel, R. J., & Leclair, S. F. (2001). Bedforms and associated sedimentary structures formed under supercritical water flows over aggrading sand beds. *Sedimentology*, *48*(1), 133-152.

Bartschi, N. C., Saylor, J. E., Lapen, T. J., Blum, M. D., Pettit, B. S., & Andrea, R. A. (2018). Tectonic controls on Late Cretaceous sediment provenance and stratigraphic architecture in the Book Cliffs, Utah. *GSA Bulletin*, *130*(11-12), 1763-1781.

Best, J. L., & Ashworth, P. J. (1997). Scour in large braided rivers and the recognition of sequence stratigraphic boundaries. *Nature*, *387*(6630), 275-277.

Bhattacharya, J. P. (1993). The expression and interpretation of marine flooding surfaces and erosional surfaces in core; examples from the Upper Cretaceous Dunvegan Formation, Alberta foreland basin, Canada. *Sequence stratigraphy and facies associations*, 125-160.

Bhattacharya, J. P. (2011). Practical problems in the application of the sequence stratigraphic method and key surfaces: integrating observations from ancient fluvial–deltaic wedges with Quaternary and modelling studies. *Sedimentology*, *58*(1), 120-169.

Blum, M. D. (1993). Genesis and architecture of incised valley fill sequences: a late Quaternary example from the Colorado River, Gulf Coastal Plain of Texas.

Blum, M. D., & Törnqvist, T. E. (2000). Fluvial responses to climate and sea-level change: a review and look forward. *Sedimentology*, *47*, 2-48.

Blum, M. D., & Aslan, A. (2006). Signatures of climate vs. sea-level change within incised valley-fill successions: Quaternary examples from the Texas Gulf Coast. *Sedimentary Geology*, *190*(1-4), 177-211.

Blum, M. D. (2013). Sediment Supply to the Shelf Margin and Beyond: Alluvial Valley Responses to Sea-Level Change.

Bull, W. B. (1991). Geomorphic responses to climatic change.

Buntin, R. C. C., Hasiotis, S. T., & Flaig, P. P. (2022). Evaluating the ichnofossil Teredolites as an indicator of salinity and paleoenvironment. *Palaios*, *37*(3), 53-72.

Burgener, L., Hyland, E., Huntington, K. W., Kelson, J. R., & Sewall, J. O. (2019). Revisiting the equable climate problem during the Late Cretaceous greenhouse using paleosol carbonate clumped isotope temperatures from the Campanian of the Western Interior Basin, USA. *Palaeogeography, Palaeoclimatology, Palaeoecology*, *516*, 244-267.

Cartigny, M. J., Ventra, D., Postma, G., & van Den Berg, J. H. (2014). Morphodynamics and sedimentary structures of bedforms under supercritical-flow conditions: new insights from flume experiments. *Sedimentology*, *61*(3), 712-748.

Chamberlin, E. P., & Hajek, E. A. (2019). Using bar preservation to constrain reworking in channel-dominated fluvial stratigraphy. *Geology*, *47*(6), 531-534.

Chamberlin, E. P., & Hajek, E. A. (2022). Fine-sediment Supply Can Control Fluvial Deposit Architecture: An Example From the Blackhawk Formation-Castlegate Sandstone Transition, Upper Cretaceous, Utah, USA. *The Sedimentary Record*, *20*(1).

Chan, M. A., & Pfaff, B. J. (1991). Fluvial sedimentology of the Upper Cretaceous Castlegate Sandstone, Book Cliffs, Utah.

Cornish, F. G. (1986). The trace-fossil Diplocraterion: Evidence of animal–sediment interactions in Cambrian tidal deposits. *PALAIOS*, *1*, 478–491.10.2307/3514630

Cross, D. B. (2016). High-frequency tectonic sequences in the Campanian Castlegate Formation during a transition from the Sevier to Laramide orogeny, Utah, U.S.A. [M.Sc. Thesis]: University of New Orleans, Paper 2133, 54 p

Curley, A. N., Petersen, S. V., Fricke, H., & Gleason, J. (2025). Insight into climate and hydrology of the late cretaceous western interior basin from clumped isotope Paleothermometry and strontium isotopes. *Earth and Planetary Science Letters*, *651*, 119180.

DeCelles, P. G., & Coogan, J. C. (2006). Regional structure and kinematic history of the Sevier fold-and-thrust belt, central Utah. *Geological Society of America Bulletin, 118*(7-8), 841-864.

Dennis, K. J., Cochran, J. K., Landman, N. H., & Schrag, D. P. (2013). The climate of the Late Cretaceous: New insights from the application of the carbonate clumped isotope

thermometer to Western Interior Seaway macrofossil. *Earth and Planetary Science Letters*, *362*, 51-65.

Distel, D. L., Amin, M., Burgoyne, A., Linton, E., Mamangkey, G., Morrill, W., Nove, J., Wood, N., & Yang, J. (2011). Molecular phylogeny of Pholadoidea Lamarck, 1809 supports a single origin for xylotrophy (wood feeding) and xylotrophic bacterial endosymbiosis in Bivalvia. *Molecular phylogenetics and evolution*, *61*(2), 245-254.

Fielding, C. R. (2006). Upper flow regime sheets, lenses and scour fills: extending the range of architectural elements for fluvial sediment bodies. *Sedimentary Geology*, *190*(1-4), 227-240.

Foley, M. G. (1977). Gravel-lens formation in antidune-regime flow; a quantitative hydrodynamic indicator. *Journal of Sedimentary Research*, *47*(2), 738-746.

Foreman, B. Z., Fricke, H. C., Lohmann, K. C., & Rogers, R. R. (2011). Reconstructing paleocatchments by integrating stable isotope records, sedimentology, and taphonomy: A Late Cretaceous case study (Montana, United States). *Palaios*, *26*(9), 545-554.

Fouch, T. D., Lawton, T. F., Nichols, D. J., Cashion, W. B., & Cobban, W. A. (1983). Patterns and timing of synorogenic sedimentation in Upper Cretaceous rocks of central and northeast Utah. Rocky Mountain Section (SEPM).

Fricke, H. C., Foreman, B. Z., & Sewall, J. O. (2010). Integrated climate model-oxygen isotope evidence for a North American monsoon during the Late Cretaceous. *Earth and Planetary Science Letters*, *289*(1-2), 11-21.

Froude, M. J., Alexander, J., Barclay, J., & Cole, P. (2017). Interpreting flash flood Paleoflow parameters from Antidunes and gravel lenses: an example from Montserrat, West Indies. *Sedimentology*, *64*, 1817–1845.

Fürsich, F. T. (1974a). On Diplocraterion Torell 1870 and the significance of morphological features in vertical, spreiten-bearing U-shaped trace fossils. *Journal of Paleontology*, *48*, 952–962.

Fürsich, F. T. (1975). Trace fossils as environmental indicators in the Corallian of England and Normandy. *Lethaia*, *8*, 151–172.10.1111/let.1975.8.issue-2

Garrison, J. R., & Van den Bergh, T. C. (2006). Effects of sedimentation rate, rate of relative rise in sea level, and duration of sea-level cycle on the filling of incised valleys: examples of filled and “overfilled” incised valleys from the Upper Ferron Sandstone, Last Chance Delta, east-central Utah, USA.

Giangrande, A., Geraci, S., & Belmonte, G. (1994). Life-cycle and life-history diversity in marine invertebrates and the implications in community dynamics. *Oceanography and Marine Biology: An Annual Review*, *32*, 305-333.

Gibling, M. R., Tandon, S. K., Sinha, R., & Jain, M. (2005). Discontinuity-bounded alluvial sequences of the southern Gangetic Plains, India: aggradation and degradation in response to monsoonal strength. *Journal of Sedimentary Research*, *75*(3), 369-385.

Gibling, M. R., Fielding, C. R., & Sinha, R. (2011). Alluvial valleys and alluvial sequences: towards a geomorphic assessment.

Goldring, R. (1962). The trace fossils of the baggy beds (upper Devonian) of North Devon, England. *Paläontologische Zeitschrift*, *36*, 232–251.10.1007/BF02986976

Goodbred Jr, S. L., & Kuehl, S. A. (1998). Floodplain processes in the Bengal Basin and the storage of Ganges–Brahmaputra river sediment: an accretion study using 137Cs and 210Pb geochronology. *Sedimentary Geology*, *121*(3-4), 239-258.

Goodbred Jr, S. L., & Kuehl, S. A. (2000). The significance of large sediment supply, active tectonism, and eustasy on margin sequence development: Late Quaternary stratigraphy and evolution of the Ganges–Brahmaputra delta. *Sedimentary Geology*, *133*(3-4), 227-248.

Goodbred Jr, S. L., Kuehl, S. A., Steckler, M. S., & Sarker, M. H. (2003). Controls on facies distribution and stratigraphic preservation in the Ganges–Brahmaputra delta sequence. *Sedimentary Geology*, *155*(3-4), 301-316.

Guccione, M. J. (1995). Indirect response of the Peace River, Florida, to episodic sea-level change. *Journal of coastal research*, 637-650.

Hajek, E. A., & Heller, P. L. (2012). Flow-depth scaling in alluvial architecture and nonmarine sequence stratigraphy: example from the Castlegate Sandstone, central Utah, USA. *Journal of Sedimentary Research*, *82*(2), 121-130.

Hampson, G. J. (2010). Sediment dispersal and quantitative stratigraphic architecture across an ancient shelf. *Sedimentology*, *v. 57*, 96–141.

Hampson, G. J., Duller, R. A., Petter, A. L., Robinson, R. A. J., & Allen, P. A. (2014). Mass balance constraints on stratigraphic interpretation of linked alluvial–coastal–shelfal deposits: example from Cretaceous Western Interior Basin, Utah and Colorado, USA. *Journal of Sedimentary Research*, *v. 84*, 935–960. doi:10.2110/jsr.2014.78

Hampson, G. J. (2016). Towards a sequence stratigraphic solution set for autogenic processes and allogenic controls: Upper Cretaceous strata, Book Cliffs, Utah, USA. *Journal of the Geological Society*, *173*(5), 817-836.

Hettinger, R. D., & Kirschbaum, M. A. (2002). *Stratigraphy of the Upper Cretaceous Mancos Shale (upper part) and Mesaverde Group in the southern part of the Uinta and Piceance basins, Utah and Colorado* (No. 2764).

Holbrook, J. M. (1996). Complex fluvial response to low gradients at maximum regression; a genetic link between smooth sequence-boundary morphology and architecture of overlying sheet sandstone. *Journal of Sedimentary Research*, *66*(4), 713-722.

Holbrook, J. (2001). Origin, genetic interrelationships, and stratigraphy over the continuum of fluvial channel-form bounding surfaces: an illustration from middle Cretaceous strata, southeastern Colorado. *Sedimentary Geology*, *144*(3-4), 179-222. doi:10.1016/S0037-0738(01)00118-X

Holbrook, J., Scott, R. W., & Oboh-Ikuenobe, F. E. (2006). Base-level buffers and buttresses: a model for upstream versus downstream control on fluvial geometry and architecture within sequences. *Journal of sedimentary research*, *76*(1), 162-174.

Holbrook, J. M. (2010). Valleys that never were: time surfaces versus stratigraphic surfaces—Discussion. *Journal of Sedimentary Research*, *80*(1), 2-3.

Holbrook, J. M., & Bhattacharya, J. P. (2012). Reappraisal of the sequence boundary in time and space: case and considerations for an SU (subaerial unconformity) that is not a sediment bypass surface, a time barrier, or an unconformity. *Earth-Science Reviews*, *113*(3-4), 271-302.

Holbrook, J., & Wanas, H. (2014). A fulcrum approach to assessing source-to-sink mass balance using channel paleohydrologic paramaters derivable from common fluvial data sets with an example from the Cretaceous of Egypt. *Journal of Sedimentary Research*, *84*(5), 349-372.

Horton, B. K., Constenius, K. N., & DeCelles, P. G. (2004). Tectonic control on coarse grained foreland-basin sequences: An example from the Cordilleran foreland basin, Utah. *Geology*, *32*(7), 637-640. doi:10.1130/G20407.1.

Howell, J. A., Eide, C. H., & Hartley, A. (2018). No evidence for significant sea level fall in the Cretaceous strata of the Book Cliffs of eastern Utah. In *AAPG ACE 2018*.

Kump, L. R., & Slingerland, R. L. (1999). Circulation and stratification of the early Turonian Western Interior Seaway: Sensitivity to a variety of forcings. *Special Paper of the Geological Society of America*, 332, 181-190.

Lane, E. W. (1956). Discussion of "The Importance of Fluvial Morphology in Hydraulic Engineering". *Journal of the hydraulics Division*, *82*(5), 1092-5.

Lang, J., & Winsemann, J. (2013). Lateral and vertical facies relationships of bedforms deposited by aggrading supercritical flows: from cyclic steps to humpback dunes. *Sedimentary Geology*, *296*, 36-54.

Lawton, T. F. (1986). Fluvial systems of the Upper Cretaceous Mesaverde Group and Paleocene North Horn Formation, central Utah: a record of transition from thin-skinned to thick-skinned deformation in the foreland region.

Leclair, S. F., & Bridge, J. S. (2001). Quantitative interpretation of sedimentary structures formed by river dunes. *Journal of Sedimentary Research*, *71*(5), 713-716.

Li, W., Bhattacharya, J. P., & Campbell, C. (2010). Temporal evolution of fluvial style in a compound incised-valley fill, Ferron "Notom Delta", Henry Mountains region, Utah (USA). *Journal of Sedimentary Research*, *80*(6), 529-549.

Li, S., Yu, X., Chen, B., & Li, S. (2015). Quantitative characterization of architecture elements and their response to base-level change in a sandy braided fluvial system at a mountain front. *Journal of Sedimentary Research*, *85*(10), 1258-1274.

Lockley, M., Hunt, A., Holbrook, J., Matsukawa, M., & Meyer, C. (1992). The dinosaur freeway: a preliminary report on the Cretaceous megatracksite, Dakota Group, Rocky Mountain front range, and high plains, Colorado, Oklahoma and New Mexico. Rocky Mountain Section (SEPM).

MacIntosh, H., de Nys, R., & Whalan, S. (2014). Contrasting life histories in shipworms: growth, reproductive development and fecundity. *Journal of Experimental Marine Biology and Ecology*, *459*, 80-86.

MacKenzie, D. B., & Poole, D. M. (1962). Provenance of Dakota group sandstones of the western interior. Wyoming Geological Association.

Mackin, J. H. (1948). Concept of the graded river: *Geological Society of America Bulletin, 59*.

Makinouchi, T., Mori, S., Danhara, T., & Takemura, K. Geologic profile WG of Research Committee for the Ground of Nohbi Plain (2001): Ages of the basal gravel of alluvium (BG) and the lower marine clay member of late Pleistocene Atsuta Formation under the Nohbi Plain, central Japan: Fruitful results based on tephra analyses of core samples recovered from the coastal area. *Journal of the Geological Society of Japan*, *107*, 283-295.

Martin, J., Paola, C., Abreu, V., Neal, J., & Sheets, B. (2009). Sequence stratigraphy of experimental strata under known conditions of differential subsidence and variable base level. *AAPG bulletin*, *93*(4), 503-533.

Mason, T. R., & Christie, A. D. M. (1986). Palaeoevironmental significance of ichnogenus Diplocraterion Torell from the Permian Vryheid formation of the Karoo Supergroup, South Africa. *Palaeogeography, Palaeoclimatology, Palaeoecology*, *52*, 249-265.10.1016/0031-0182(86)90050-7

McLaurin, B. T., & Steel, R. J. (2000). Fourth-order nonmarine to marine sequences, middle Castlegate Formation, Book Cliffs, Utah. *Geology*, *28*(4), 359-362.

McLaurin, B. T., & Steel, R. J. (2007). Architecture and origin of an amalgamated fluvial sheet sand, lower Castlegate Formation, Book Cliffs, Utah. *Sedimentary Geology*, *197*(3-4), 291-311.

Miall, A. D. (1985). Architectural-element analysis: A new method of facies analysis applied to fluvial deposits. *Earth-science reviews*. *22*(4), 261-308. doi:10.1016/0012-8252(85)90001-7

Miall, A. D. (1988). Reservoir heterogeneities in fluvial sandstones: lessons from outcrop studies. *AAPG bulletin*, *72*(6), 682-697.

Miall, A. D. (1993). The architecture of fluvial-deltaic sequences in the upper Mesaverde Group (Upper Cretaceous), Book Cliffs, Utah. *Geological Society, London, Special Publications*, *75*(1), 305-332.

Miall, A. D. (1994). Reconstructing fluvial macroform architecture from two-dimensional outcrops; examples from the Castlegate Sandstone, Book Cliffs, Utah. *Journal of Sedimentary Research*, *64*(2b), 146-158.

Miall, A.D. (1996). The stratigraphic architecture of fluvial depositional systems. *The Geology of Fluvial Deposits: Sedimentary Facies, Basin Analysis, and Petroleum Geology*, 251-309.

Miall, A. D., & Arush, M. (2001). The Castlegate Sandstone of the Book Cliffs, Utah: sequence stratigraphy, paleogeography, and tectonic controls. *Journal of Sedimentary Research*, *71*(4), 537-548.

Miall, A. D., & Arush, M. (2001). Cryptic sequence boundaries in braided fluvial successions. *Sedimentology*, *48*(5), 971-985.

Miall, A. (2014). The emptiness of the stratigraphic record: a preliminary evaluation of missing time in the Mesaverde Group, Book Cliffs, Utah, USA. *Journal of Sedimentary Research*, *84*(6), 457-469. doi:10.2110/jsr.2014.40

Miall, A. D. (2016). The valuation of unconformities. *Earth-Science Reviews*, *163*, 22-71.

Milana, J. P., & Tietze, K. W. (2002). Three-dimensional analogue modelling of an alluvial basin margin affected by hydrological cycles: processes and resulting depositional sequences. *Basin Research*, *14*(3), 237-264.

Miller, I. M., Johnson, K. R., Kline, D. E., Nichols, D. J., & Barclay, R. S. (2013). A Late Campanian flora from the Kaiparowits Formation, southern Utah, and a brief overview of the widely sampled but little-known Campanian vegetation of the Western Interior of North America. *At the top of the grand staircase: The Late Cretaceous of Southern Utah*, 107-131. Indiana University Press. http://www.jstor.org/stable/j.ctt16gzhs1.13

Mitten, A. J., Howell, L. P., Clarke, S. M., & Pringle, J. K. (2020). Controls on the deposition and preservation of architectural elements within a fluvial multi-storey sandbody. *Sedimentary Geology, 401*, 105629. https://doi.org/10.1016/j.sedgeo.2020.105629

Nair, N. B., & Saraswathy, M. (1971). The biology of wood-boring teredinid molluscs. In Advances in marine biology (Vol. 9, pp. 335-509). *Academic Press*.

Oloriz, F., & Rodriguez-Tovar, F. J. (2000). Diplocraterion: A useful marker for sequence stratigraphy and correlation in the Kimmeridgian, Jurassic (Prebetic Zone, Betic Cordillera, southern Spain). *PALAIOS*, *15*, 546–552.

Olsen, T., Steel, R., Hogseth, K., Skar, T., & Roe, S. L. (1995). Sequential architecture in a fluvial succession; sequence stratigraphy in the Upper Cretaceous Mesaverde Group, Prince Canyon, Utah. *Journal of Sedimentary Research*, *65*(2b), 265-280.

Paola, C., & Mohrig, D. (1996). Palaeohydraulics revisited: Palaeoslope estimation in coarse grained braided rivers. *Basin Research, 8*(3), 243-254. https://doi.org/10.1046/j.1365-2117.1996.00253.x

Paola, C. (2000). Quantitative models of sedimentary basin filling. *Sedimentology*, *47*, 121-178.

Pattison, S. A. (2018). Rethinking the incised-valley fill paradigm for Campanian Book Cliffs strata, Utah–Colorado, USA: evidence for discrete parasequence-scale, shoreface incised channel fills. *Journal of Sedimentary Research*, *88*(12), 1381-1412.

Pattison, S. A. (2019). High resolution linkage of channel-coastal plain and shallow marine facies belts, Desert Member to Lower Castlegate Sandstone stratigraphic interval, Book Cliffs, Utah-Colorado, USA. *GSA Bulletin*, *131*(9-10), 1643-1672.

Pattison, S. A. (2020). Sediment-supply-dominated stratal architectures in a regressively stacked succession of shoreline sand bodies, Campanian Desert member to Lower Castlegate Sandstone interval, Book Cliffs, Utah–Colorado, USA. *Sedimentology*, *67*(1), 390-430. doi:10.1111/sed.12647

Pattison, S. A. (2020). No evidence for an unconformity at the base of the lower Castlegate Sandstone in the Campanian Book Cliffs, Utah–Colorado, United States: Implications for sequence stratigraphic models. *AAPG Bulletin*, *104*(3), 595-628. https://doi.org/10.1306/07151918158

Petter, A. L. (2010). Stratigraphic implications of the spatial and temporal variability in sediment transport in rivers, deltas, and shelf margins. The University of Texas at Austin.

Pettit, B. S., Blum, M., Pecha, M., McLean, N., Bartschi, N. C., & Saylor, J. E. (2019). Detrital-Zircon U-PB Paleodrainage reconstruction and Geochronology of the Campanian Blackhawk–Castlegate succession, Wasatch plateau and book cliffs, Utah, USA. *Journal of Sedimentary Research*, *89*(4), 273-292. https://doi.org/10.2110/jsr.2019.18

Plink-Björklund, P. (2015). Morphodynamics of rivers strongly affected by monsoon precipitation: review of depositional style and forcing factors. *Sedimentary Geology*, *323*, 110-147.

Posamentier, H. W. (2001). Lowstand alluvial bypass systems: incised vs. unincised. *AAPG bulletin*, *85*(10), 1771-1793.

Postma G. (1997). The geology of fluvial deposits, sedimentary facies, basin analysis and petroleum geology: Andrew D. Miall. *Sedimentary Geology*, *110*(1),149-150. doi:10.1016/S0037-0738(96)00081-4

Poulsen, C. J., Barron, E. J., Johnson, C. C., & Fawcett, P. (1999). Links between major climatic factors and regional oceanic circulation in the mid-Cretaceous.

Poulsen, C. J., Pollard, D., & White, T. S. (2007). General circulation model simulation of the δ18O content of continental precipitation in the middle Cretaceous: A model-proxy comparison. *Geology*, *35*(3), 199-202.

Rittenour, T. M., Blum, M. D., & Goble, R. J. (2007). Fluvial evolution of the lower Mississippi River valley during the last 100 ky glacial cycle: Response to glaciation and sea-level change. *Geological Society of America Bulletin*, *119*(5-6), 586-608.

Robinson, R. A., & Slingerland, R. L. (1998). Grain-size trends, basin subsidence and sediment supply in the Campanian Castlegate Sandstone and equivalent conglomerates of central Utah. *Basin Research*, *10*(1), 109-127.

Rodríguez-Tovar, F. J., & Pérez-Valera, F. (2013). Variations in population structure of Diplocraterion parallelum: Hydrodynamic influence, food availability, or nursery settlement? *Palaeogeography, Palaeoclimatology, Palaeoecology*, *369*, 501–509.

Seilacher, A. (2007). *Trace fossil analysis* (272 p). Berlin: Springer.

Seymour, D. L., & Fielding, C. R. (2013). High resolution correlation of the Upper Cretaceous stratigraphy between the Book Cliffs and the western Henry Mountains Syncline, Utah, USA. *Journal of Sedimentary Research*, *83*(6), 475-494. doi:10.2110/jsr.2013.37

Shanley, K. W., & McCabe, P. J. (1994). Perspectives on the sequence stratigraphy of continental strata. *AAPG bulletin*, *78*(4), 544-568.

Slootman, A., De Boer, P. L., Cartigny, M. J., Samankassou, E., & Moscariello, A. (2019). Evolution of a carbonate delta generated by gateway-funnelling of episodic currents. *Sedimentology*, *66*(4), 1302-1340.

Slootman, A., & Cartigny, M. J. (2020). Cyclic steps: review and aggradation-based classification. *Earth-Science Reviews*, *201*, 102949.

Slootman, A., Vellinga, A. J., Moscariello, A. and Cartigny, M. J. B. (2021). The depositional signature of high-aggradation chute-and-pool bedforms: the build-and-fill structure. *Sedimentology*, *68*, 1640–1673.

Strong, N., & Paola, C. (2008). Valleys that never were: time surfaces versus stratigraphic surfaces. *Journal of Sedimentary Research*, *78*(8), 579-593.

Sundell, K. E., Gehrels, G. E., D. Blum, M., Saylor, J. E., Pecha, M. E., & Hundley, B. P. (2024). An exploratory study of "large-n" detrital zircon geochronology of the Book Cliffs, UT via rapid (3 s/analysis) U–Pb dating. *Basin Research*, *36*(1), e12840. doi:10.1111/bre.12840

Sylvia, D. A., & Galloway, W. E. (2006). Morphology and stratigraphy of the late Quaternary lower Brazos valley: Implications for paleo-climate, discharge and sediment delivery. *Sedimentary Geology*, *190*(1-4), 159-175.

Törnqvist, T. E. (1998). Longitudinal profile evolution of the Rhine–Meuse system during the last deglaciation: interplay of climate change and glacio-eustasy?. *Terra Nova*, *10*(1), 11-15.

Törnqvist, T. E., Wallinga, J., Murray, A. S., De Wolf, H., Cleveringa, P., & De Gans, W. (2000). Response of the Rhine–Meuse system (west-central Netherlands) to the last Quaternary glacio-eustatic cycles: a first assessment. *Global and Planetary Change*, *27*(1-4), 89-111.

Trampush, S. M., Huzurbazar, S., & McElroy, B. (2014). Empirical assessment of theory for bankfull characteristics of alluvial channels. *Water Resources Research*, *50*(12), 9211-9220. https://doi.org/10.1002/2014WR015597

Trower, E. J., Ganti, V., Fischer, W. W., & Lamb, M. P. (2018). Erosional surfaces in the Upper Cretaceous Castlegate Sandstone (Utah, USA): Sequence boundaries or autogenic scour from backwater hydrodynamics?. *Geology*, *46*(8), 707-710. https://doi.org/10.1130/G40273.1

Van de Graaff, F. R. (1972). Fluvial--deltaic facies of the Castlegate Sandstone (Cretaceous), east-central Utah. *Journal of Sedimentary Research*, *42*(3). doi:10.1306/74D725B8-2B21-11D7-8648000102C1865D.

Van Den Berg, A. P. H., Saparoea, V., & Postma, G. (2008). Control of climate change on the yield of river systems.

Van Wagoner, J. C., Mitchum, R. M., Campion, K. M., and Rahmanian, V. D. (1990). Siliciclastic Sequence Stratigraphy in Well Logs, Cores, and Outcrops. *American Association of Petroleum Geologists*, *Methods in Exploration Series 7*, 1-55.

Van Wagoner, J. C. (1991). Sequence stratigraphy and facies architecture of the Desert Member of the Blackhawk Formation and the Castlegate Formation in the Book Cliffs of eastern Utah and western Colorado, in Van Wagoner, J.C., Nummedal, D., Jones, C.R., Taylor, D.R., Jennette, D.C., and Riley, G.W., eds., Sequence Stratigraphy Applications to Shelf Sandstone Reservoirs: Outcrop to Subsurface Examples. *American Association of Petroleum Geologists*, *Field Conference Guidebook*.

Van Wagoner, J. C. (1995). Sequence stratigraphy and marine to nonmarine facies architecture of foreland basin strata, Book Cliffs, Utah, U.S.A., in Van Wagoner, J.C., and Bertram, G.T., eds., Sequence Stratigraphy of Foreland Basin Deposits: Outcrop and Subsurface Examples from the Cretaceous of North America. *American Association of Petroleum Geologists*, *Memoir 64*, 137–223.

van Yperen, A. E., Line, L. H., Holbrook, J. M., More, M. P., & Midtkandal, I. (2019). Revised stratigraphic relationships of the Dakota Group in the Tucumcari Basin, San Miguel County, New Mexico, USA. In *New Mexico Geological Society Guidebook, 70th Field Conference, Geology of the Raton-Clayton Area* (pp. 89-100). New Mexico Geological Society.

van Yperen, A. E., Holbrook, J. M., Poyatos-Moré, M., Myers, C., & Midtkandal, I. (2021). Low-accommodation and backwater effects on sequence stratigraphic surfaces and depositional architecture of fluvio-deltaic settings (Cretaceous Mesa Rica Sandstone, Dakota Group, USA). *Basin Research*, *33*(1), 513-543. doi:10.1111/bre.12483

van Yperen, A. E., Holbrook, J. M., Poyatos-Moré, M., & Midtkandal, I. (2024). Backwater length estimates in modern and ancient fluvio-deltaic settings: Review and proposal of standardized workflows. *Earth-Science Reviews*, *250*, 104692.

Voight, J. R. (2015). Xylotrophic bivalves: aspects of their biology and the impacts of humans. *Journal of Molluscan Studies*, *81*(2), 175-186.

Wallinga, J., Törnqvist, T. E., Busschers, F. S., & Weerts, H. J. (2004). Allogenic forcing of the late Quaternary Rhine–Meuse fluvial record: the interplay of sea-level change, climate change and crustal movements. *Basin Research*, *16*(4), 535-547.

Wang, J., & Plink-Björklund, P. (2019). Stratigraphic complexity in fluvial fans: Lower Eocene Green River Formation, Uinta Basin, USA. *Basin Research*, *31*(5), 892-919.

Weissmann, G. S., Mount, J. F., & Fogg, G. E. (2002). Glacially driven cycles in accumulation space and sequence stratigraphy of a stream-dominated alluvial fan, San Joaquin Valley, California, USA. *Journal of Sedimentary Research*, *72*(2), 240 251.

Weissmann, G. S., Bennett, G. L., & Lansdale, A. L. (2005). Factors controlling sequence development on Quaternary fluvial fans, San Joaquin Basin, California, USA.

Wellner, R. W., & Bartek, L. R. (2003). The effect of sea level, climate, and shelf physiography on the development of incised-valley complexes: a modern example from the East China Sea. *Journal of sedimentary research*, *73*(6), 926-940.

Willis, A. (2000). Tectonic control of nested sequence architecture in the Sego Sandstone, Neslen Formation and upper Castlegate Sandstone (Upper Cretaceous), Sevier foreland basin, Utah, USA. *Sedimentary Geology*, *136*(3-4), 277-317.

Yoshida, S., Willis, A., & Miall, A. D. (1996). Tectonic control of nested sequence architecture in the Castlegate Sandstone (upper Cretaceous), Book Cliffs, Utah. *Journal of Sedimentary Research*, *66*(4), 737-748.

Yoshida, S., Miall, A. D., & Willis, A. (1998). Sequence stratigraphy and marine to nonmarine facies architecture of foreland basin strata, Book Cliffs, Utah, USA: Discussion. *AAPG bulletin*, *82*(8), 1596-1606.

Yoshida, S. (2000). Sequence and facies architecture of the upper Blackhawk formation and the lower Castlegate Sandstone (Upper Cretaceous), Book Cliffs, Utah, USA. *Sedimentary Geology*, *136*(3-4), 239-276.

VITA

Personal Background	Brayton Lee Keith Anchorage, Alaska Son of Brian Lee and Tanya Marie Keith
Education	Diploma, East Anchorage High School Anchorage, Alaska, 2015 Bachelor of Science, Geology, University of Alaska, Anchorage, 2021
Experience	Geology Intern, State of Alaska DGGS Anchorage, Alaska, 2018-2021 Geologist 1, State of Alaska DGGS Anchorage, Alaska, 2022 Geologist, Alaska Earth Sciences Anchorage, Alaska, 2022 Graduate Teaching Assistant, Texas Christian University, Fort Worth, 2022-2024 Geoscience Intern, Devon Energy Oklahoma City, Oklahoma, 2024
Professional Memberships	Society for Sedimentary Geology American Association of Petroleum Geologists

ABSTRACT

FLUVIAL ARCHITECTURE ANALYSIS AND LONGITUDINAL VARIANCE OF THE CASTLEGATE SANDSTONE, BOOK CLIFFS, UTAH

By Brayton Keith, M.S., 2025

Department of Geological Sciences

Texas Christian University

Thesis Advisor: John Holbrook, Professor of Geology

The Castlegate Sandstone is one of the most-studied fluvial deposits in the world due to its world-class exposure. Despite this, there has yet to be a comprehensive fluvial architecture analysis study considering the longitudinal variance within the system. This study uses methods of lithofacies analysis, analysis of fluvial architectural elements, and calculation of backwater length to reconstruct the depositional history of the Castlegate Sandstone. This study recognizes valley-scale scours in the Castlegate, a frequently overlooked surface within the hierarchy of fluvial bounding surfaces. Data collected was compared and supplemented with the numerous previous studies on this rock unit. This study determines the lack of trackable surfaces from the proximal to distal reaches of the Castlegate system due to the different controls on fluvial architecture in different regions of the system, and provides insight into driving factors of change in fluvial architecture and channel style along longitudinal profile.